Satellite ocean-colour remote sensing of the South Taranaki Bight from 2002 to 2012

Prepared for Trans-Tasman Resources Ltd

October 2013

Authors/Contributors:
Matt Pinkerton
Jill Schwarz
Mark Gall
Jenny Beaumont

For any information regarding this report please contact:
Matt Pinkerton
Principal Scientist
Ocean Atmosphere
+64-4-386 0300
m.pinkerton@niwa.co.nz

National Institute of Water & Atmospheric Research Ltd
301 Evans Bay Parade, Greta Point
Wellington 6021
Private Bag 14901, Kilbirnie
Wellington 6241
New Zealand

Phone +64-4-386 0300
Fax +64-4-386 0574

NIWA Client Report No: WLG2013-14 Rev 1
Report date: October 2013
NIWA Project: TTR11301

Cover image: Satellite image of the South Taranaki Bight 29 April 2011

© All rights reserved. This publication may not be reproduced or copied in any form without the permission of the copyright owner(s). Such permission is only to be given in accordance with the terms of the client's contract with NIWA. This copyright extends to all forms of copying and any storage of material in any kind of information retrieval system.

Whilst NIWA has used all reasonable endeavours to ensure that the information contained in this document is accurate, NIWA does not give any express or implied warranty as to the completeness of the information contained herein, or that it will be suitable for any purpose(s) other than those specifically contemplated during the Project or agreed by NIWA and the Client.

Contents

Tables

Figures

Reviewed by Alison MacDiarmid

Approved for release by Julie Hall

……

……

Executive summary

Trans-Tasman Resources Ltd. (TTR) proposes to mine iron sands in the South Taranaki Bight (STB), approximately 22–40 km from the coast in water depths of 25–45 m. Dredging seafloor sediments, and deposition of tailings will produce down-current plumes of suspended sediments that may significantly alter the properties of coastal waters and levels of primary production. Baseline information on phytoplankton, suspended sediments and river run-off in the STB is needed to assess potential ecological impacts of the proposed activity.

Coastal waters exhibit high natural variability in their characteristic properties, both spatially and seasonally. Observations of the ocean from optical sensors on satellites can complement measurements of water properties from boats and moorings and provide synoptic distributions of these properties in the near-surface zone (surface to first attenuation depth), over large areas, at daily or longer timescales. Local validation and tuning of processing methods is required to use satellite observations. This study included water sampling in the STB to determine the concentrations of coloured material: phytoplankton (algae), non-algal particles including suspended sediment, and coloured dissolved organic matter, and their inherent optical properties. These in-water measurements were used to assess and develop 'locally-tuned' satellite processing methods for the STB region. These locally-tuned algorithms were applied to ten years (2002–2012) of satellite observations from the NASA MODIS-Aqua sensor in order to assess mean conditions and characterise variability of water constituents. This project also potentially acts as a precursor to using satellite data to observe changes in water quality in the region.

A summary of the key findings are:

1. The STB region is a dynamic and optically-complex environment. Turbid water processing of MODIS data was carried out using the NIR/SWIR switching atmospheric correction algorithm, the Quasi-Analytical Algorithm update 5, and locally-derived and/or validated conversions between inherent optical properties and geophysical properties. End-to-end comparisons between *in situ* and satellite observations of chlorophyll-a (chl-a) concentration (a proxy for phytoplankton biomass), total suspended matter (TSM) concentration and absorption by coloured dissolved organic matter (CDOM) in the STB indicate that the satellite data presented in this study are fit for purpose. However, satellite data are inherently less accurate than *in situ* measurements and uncertainties in individual measurements of >50% are possible.

2. Annual median concentration of TSM between the coast and 10 km offshore in the STB was 1.4 g m^{-3} (interquartile range of 0.5–5.5 g m^{-3}). Median TSM concentration decreases rapidly with distance offshore. In the region of the STB between 10 and 40 km offshore, monthly median TSM concentrations were 0.2–0.7 g m^{-3}. Between 0 and 10 km from the coast, TSM was greater than 3 g m^{-3} about 27% of the time on average (between 12% and 40% by month). Further offshore, TSM was greater than 3 g m^{-3} rarely (less than 5% of the time). There was substantial small-area and short term variability in TSM from satellite maps that is associated with river plumes, local resuspension of sediment and/or coastal erosion. There is evidence in individual

satellite images of plumes with relatively high concentrations of sediment (>4 g m^{-3}) being transported more than 30 km offshore.

3. Elevated chl-a concentrations in the STB seem to be associated with two processes. (a) Riverine run-off brings nutrients (nitrate, phosphate) into the STB and the nutrients stimulate phytoplankton production close to the coast where TSM concentrations are elevated. This process leads to chl-a concentration in the satellite data being positively correlated with TSM concentration. Long-term median chl-a concentrations were highest (~5 mg m^{-3}) within a few km of the coast, and rapidly decreased with distance offshore to an annual median of 0.2 mg m^{-3}. (b) More than 10 km offshore, the STB was characterized by intermittent phytoplankton blooms. These offshore blooms varied in size, but were often spatially large and sometimes covered much of the offshore STB. Some blooms may be associated with upstream Farewell Spit dynamics (e.g. Figure 11-1, Figure 11-2, Figure 11-3) and, more rarely, some may be affected by Cook Strait dynamics (Figure 11-4). Both nearshore and offshore blooms could be intense, with chl-a concentrations exceeding 4 mg m^{-3}.

4. Median absorption due to CDOM at wavelength of 412 nm (blue) was highest within a few km of the shore (>0.5 m^{-1}), decreasing to a median value of about 0.05 m^{-1} further than about 10 km from the coast. Elevated absorption by CDOM was associated predominantly with elevated TSM.

5. Based on the satellite data, at 5 selected sites there has been no long-term increase or decrease in total suspended matter or chl-a during the period 2002 to 2012.

6. The mean euphotic zone depth during the biogeo-optical sampling was ~25 m. This represents the depth above which addition of sediments would impact upon the underwater light climate and therefore potentially affect phytoplankton productivity.

7. Although not part of this contract, pseudo-true colour satellite images provide valuable spatial context to sampling campaigns and are useful in assessing the potential visual-effects of mining operations.

1 Introduction

1.1 Background

Trans-Tasman Resources Ltd (TTR) proposes to mine iron sands in the South Taranaki Bight (STB, Figure 1-1)[1], approximately 22-40 km offshore in water depths of 25-45 m. Dredging seafloor sediments and deposition of discarded tailings will produce down-current plumes of suspended sediments (Hadfield 2013). This has the potential to alter water colour and clarity, with environmental and management implications (Davies-Colley et al., 2003) for primary production and phytoplankton biomass (food-chain processes), and sighted organisms. As part of an environmental impact assessment for this proposed activity, TTR has engaged NIWA to use data from earth-observing ocean colour satellite sensors to provide information on material naturally occurring in the water column in the region potentially affected by the proposed activity. The potential impacts of sediment plumes from mining activities (or their surface expression) can then be assessed against this natural variability. Development of a remote sensing capability for observing optical water quality in the STB may also be useful for monitoring mining sediment plumes as required in the future.

Water currents in the STB are strongly influenced by the tidal currents and the prevailing westerly winds, which are modified near shore by variable river outflows (Bowman et al., 1983). Local oceanographic processes determine the distribution and fate of material in the STB. The water column may be stratified (formed of overlying layers of different densities due to temperature and salinity variations) or well-mixed between the sea-surface and sea-bed (Bowman et al., 1983). Because of the dynamic nature of oceanographic and hydrological processes introducing, transporting, transforming and removing coloured material in coastal waters, water sampling from vessels or moorings has limited ability to assess or monitor large-scale patterns (100s of km) over long periods (decades). Instead, satellite ocean colour data can be used to observe coloured material in coastal regions on appropriate time and space scales. The main coloured material in coastal waters – phytoplankton, sediment and other non-algal particulate material, and coloured dissolved organic matter (CDOM) – have different optical (absorbing and scattering) properties (Jerlov, 1974; Morel & Prieur, 1977; Mobley, 1994) and hence affect the colour of water in different ways. By measuring the colour of the water from sensors on earth-orbiting satellites it is possible to map the distributions of these components in a near-synoptic way, over large areas, at a high frequency (up to daily should clear skies allow). Compiling data over periods of years allows average seasonal, annual and inter-annual variability in the concentrations of these coloured water constituents to be provided in regions of interest or at site-specific locations.

[1] For the purposes of this report the South Taranaki Bight (STB) is defined in Figure 1-1

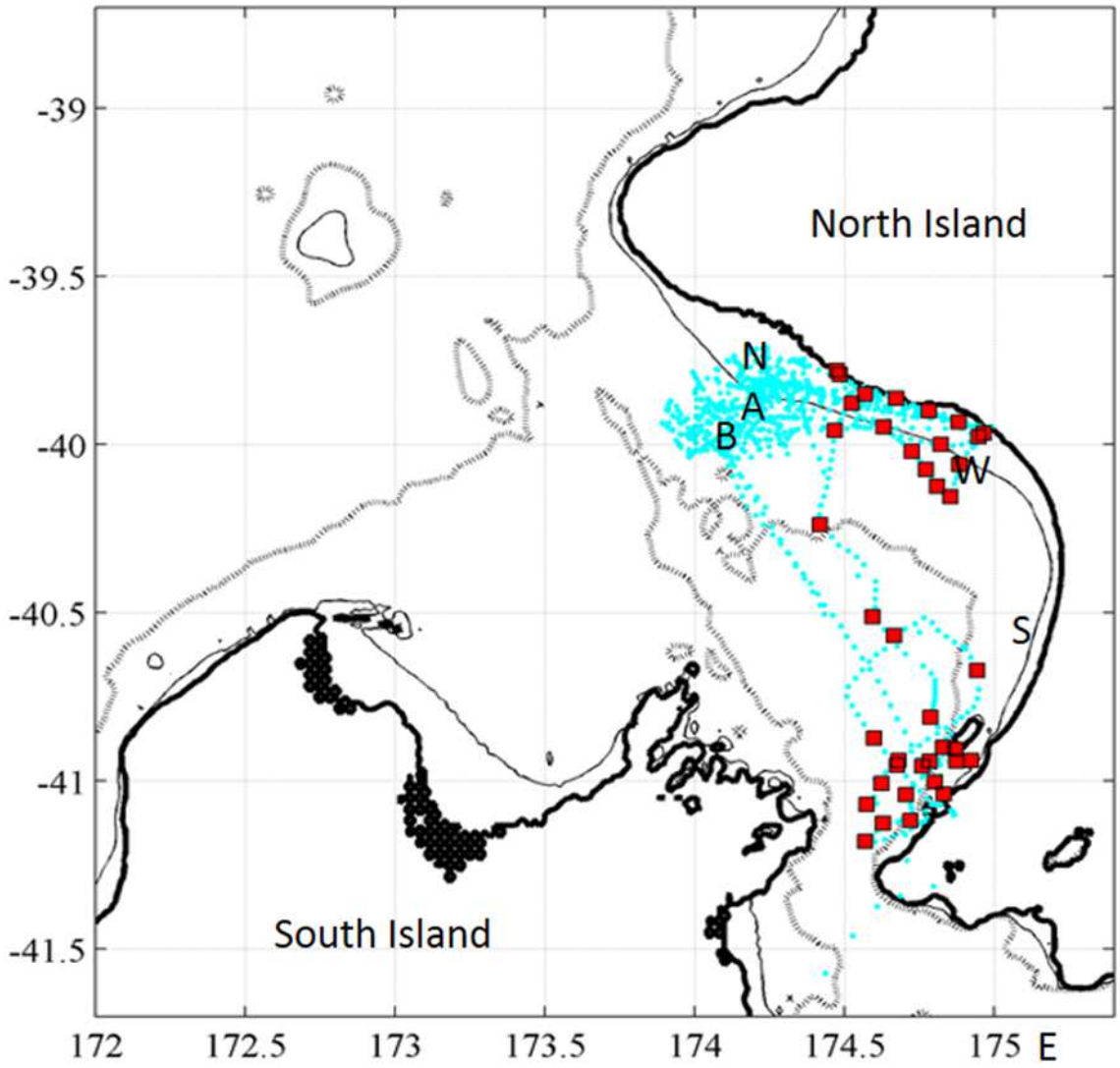

Figure 1-1: Study area of the South Taranaki Bight (STB). Discrete *in situ* sample locations (red squares) and underway track of the R.V. Ikatere (subsampled every 5 minutes, blue dots) are shown. The 30 m and 100 m isobaths are shown as solid and dotted black lines, respectively. Satellite data were extracted at five illustrative sites: A = Inner end of mining site; B = Outer end of mining site; N, S =Northern and Southern coastal sites; W=Wanganui River mouth.

1.2 Coloured water constituents

What we observe as the colour and clarity of natural waters (apparent optical properties) arise from the inherent optical properties (IOPs, absorption and scattering) of water itself, its solutes (dissolved substances) and suspended particulates, and the direction, wavelength and intensity of the incident sunlight illumination (Kirk, 2011). Optically active components are grouped depending on methodological determination: total suspended matter concentration (TSM) encompasses all mass captured by the gravimetric technique; Phytoplankton or algae are typically represented by the concentration of its major photosynthetic pigment chlorophyll-*a* (chl-a); non-algal particles (NAP) represent mineral

sediments and particulate detritus – organic breakdown products) measured after removing pigments; coloured dissolved organic matter (CDOM) is the remaining colour once all the particulates have been removed by filtering at 0.2 μm (see Section 2 for methods). Data from ocean colour satellites is typically used to map coloured material in the surface water in these three categories:

(1) **Total suspended matter (TSM)** – includes all suspended organic and inorganic particulates. Non-algal particles (NAP) in the water column are a complex mixture of living and non-living material arising from local production processes within the water column (autochthonous) and material brought in from elsewhere (allochthonous). NAP can be introduced to the water column in river water, by shore erosion and/or by re-suspension of sediment from the sea-bed. The terrigenous particulate material includes both refractory (mineral) sediment particles and organic detritus. Over timescales of a few days, phytoplankton die, are grazed by zooplankton, and/or are degraded by viral and bacterial lysis. These degradation processes lead to local formation of particulate organic matter and CDOM, the former of which forms part of the non-algal particle assemblage. Small zooplankton, bacteria and viruses also form part of non-algal particle matter in the water column. Naturally occurring TSM in the region hence contains both organic and inorganic particulates.

(2) **Phytoplankton** - Phytoplankton growth forms algal cells in the upper water column by photosynthesis. Primary production requires inter alia the presence of nutrients (principally nitrate and phosphate) naturally occurring in sea-water or introduced into the coastal zone by riverine input. Different species of phytoplankton occur in the STB which contain various mixtures of pigments - the coloured chemicals which phytoplankton use to absorb light. However, as all phytoplankton contain chlorophyll-a (chl-a), which is the dominant pigment in terms of absorption, spectral signatures are similar. Therefore, phytoplankton abundance in marine environments is quantified and mapped using the proxy of the concentration of chl-a (hereafter denoted chl-a) and measured in units of mgchl-a m^{-3}. Although chl-a is a convenient biomarker for phytoplankton biomass, the ratio between total phytoplankton biomass and chlorophyll varies between species of phytoplankton (e.g., Falkowski & Raven 1997; Kirk, 2011) and in response to light acclimation and nutrient limitation (Geider et al. 1997; Macintyre et al. 2002).

(3) **Coloured dissolved organic matter (CDOM)** – CDOM is a complex mixture of humic and fulvic acids formed by the natural breakdown of organic material in soil or aquatic environments. CDOM in the study region will occur from (1) the local breakdown of phytoplankton, zooplankton and other living material; and (2) CDOM of terrigineous origin (allochthanous) introduced to the STB from riverine sources. CDOM from these two sources tend to be optically similar. The shape of the absorption spectrum of CDOM is also typically similar to that of NAP, being highest in the blue and decreasing to the red end of the visible spectrum.

1.3 Remote sensing of ocean colour

Top-of-atmosphere satellite data must be calibrated and corrected for atmospheric absorption and scattering. In the blue and green, about 80–95% of the signal received by a radiometric sensor at the top of the atmosphere is from the atmosphere (Gordon, 1997). In order to obtain the colour of the water, and hence estimate water constituents, it is necessary

to remove the contribution from atmospheric scattering. Waters with low concentrations of suspended particulates are black in the near infra-red because of the high absorption by pure water of these wavelengths. Atmospheric correction takes advantage of this fact to estimate the contribution from the atmosphere. In coastal waters, this method fails because suspended sediments reflect light at NIR wavelengths out of the water. In oceanic water, it can be assumed that phytoplankton and their associated exudations and breakdown substances are the main drivers of changing water colour, but this is generally not true for coastal waters, where riverine input, resuspension and land erosion introduces sediment and CDOM from elsewhere. Hence, methods that correct for atmospheric radiance at the top of the atmosphere, whilst allowing for non-zero water leaving radiance in the near infra-red, are required for remote sensing in coastal regions (e.g. Lavender et al., 2005; Wang & Shi, 2007).

Although a simple, empirical algorithm relating the blue to green ratio of normalised water leaving radiance to chl-a is accurate to within about 30-40% in open ocean waters at the global scale (O'Reilly et al., 1998), there can be significantly greater uncertainty locally, especially in coastal waters (Pinkerton et al., 2005). Similarly, the accuracy of band ratio algorithms for TSM and other products depend on assumed relationships between IOPs. Semi-analytical algorithms address these issues by de-convolving remotely sensed reflectance spectra simultaneously into contributions by all potential optically active constituents, but still assume typical spectral shapes for the absorption and scattering properties of phytoplankton, dissolved substances and inorganic particulates (Garver & Siegel, 1997; Lee et al., 2002). Variations in the particular IOPs in different regions can lead to errors in semi-analytical inversion algorithms. Because it is not possible to determine *a priori* which algorithm performs best in any given region, biogeo-optical data can be collected and used to select and, if necessary, locally tune in-water algorithms.

1.4 Objectives

This study had five objectives:

1. Measure the biogeo-optical and biogeochemical properties of surface water in the South Taranaki Bight (STB)
2. Use local *in situ* measurements to select and satellite data products in the STB, including, if necessary, local tuning of the algorithms using *in situ* data.
3. Assess the distribution and concentrations of total suspended matter (TSM) over the past decade in the STB;
4. Assess the distribution and concentrations of phytoplankton biomass via the proxy of near-surface chlorophyll-a concentration (chl-a) over the past decade in the STB;
5. Assess the distribution of coloured dissolved organic matter (CDOM) over the past decade in the STB.

1.5 Structure of report

In Section 2, this report details local measurements of biogeo-optical and biogeo-chemical parameters in the STB. Section 3 reports on the use of these measurements to validate and

locally tune ocean colour processing algorithms. Sections 4 to 6 present satellite ocean colour observations of the STB for the three products of objectives 2–4 (total suspended matter, TSM; phytoplankton biomass via the proxy of near-surface chlorophyll-a concentration (chl-a); absorption by CDOM). In each section 4–6, the satellite data are used to describe the present and recent-historical state of water quality in this region, in context to its spatial and temporal variability. Section 7 discusses and summarizes the results. Appendix A shows the number of valid pixels used in the climatological satellite data analysis. Appendix B shows satellite images of individual days, selected to illustrate different conditions and processes.

2 Collection and analysis of *in situ* data

2.1 Field sampling campaigns

Waters of contrasting turbidity were targeted on four field campaigns undertaken using the *R.V. Ikatere* (Figure 1-1).

- Campaign 1: Summer – 6th to 13th December 2011.
- Campaign 2: Summer – 23rd to 30th January 2012.
- Campaign 3: Winter – 12th to 13th June 2012.
- Campaign 4: Winter – 1st to 2nd July, 2012.

Sampling was carried out in two clusters, one to the north and one in the mid/south-STB ('Mana') (Figure 1-1). Sampling near Mana allowed more stations to be visited because transits were shorter and fieldwork less affected by poor weather. The biogeo-optical properties of optically-active material occurring in the two regions were indistinguishable (see Section 2.5 below).

The voyage tracks are shown on pseudo-true colour satellite images taken close to the field sampling in Figure 2-1. Persistent cloud cover obscured the satellite view during the first voyage. The earliest clear image after the first voyage (21st December) shows blue waters off-shore and sediment plumes extending off the shelf in the northern Taranaki Bight. Only one clear image was obtained during the January voyage. Coastal waters in the northern water were characterised by bright waters typical of suspended sediments (relatively high backscatter). Conditions during the June voyage were typical of strong wind and wave-driven resuspension of sediments, as well as extremely dense sediment plumes extending off-shore from the entire Taranaki coast. Although no clear imagery was obtained during the July sampling period, conditions two weeks after the voyage were similar to the turbid conditions found during June. No sampling was carried out in spring or autumn, and it is likely that extreme high winds and/or high river flows were not sampled.

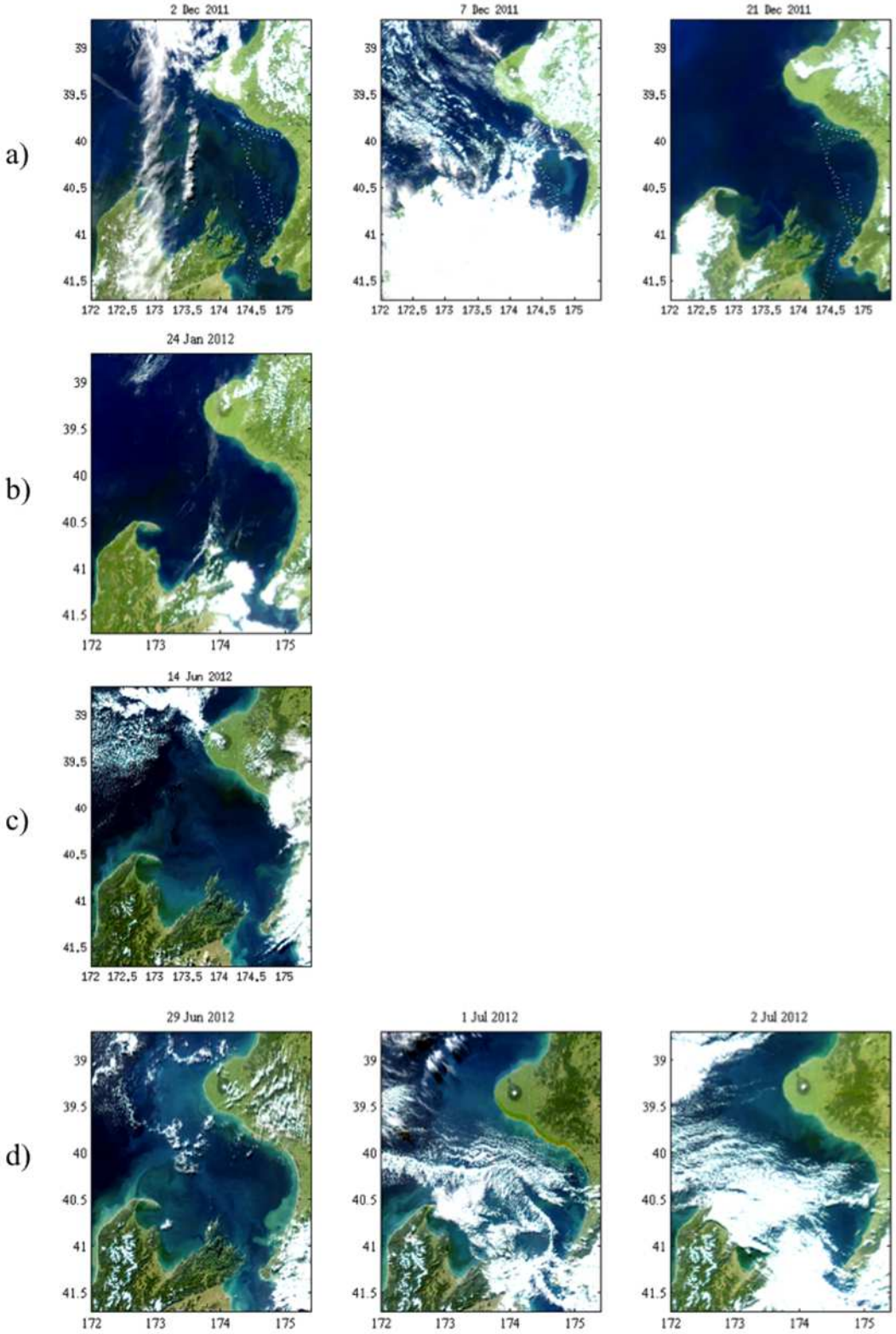

Figure 2-1: Pseudo-true colour MODIS-Aqua composites from the four *in situ* sampling periods. Voyage tracks are overlaid in a) white; b) no data; c) red; d) red. True colour composite images were generated at 250 x 250 m resolution using the SeaDAS l1mapgen program, with an upper reflectance limit of 0.2 to enhance features in the water. MODIS bands 1, 3, 4 were used.

2.2 Water sampling and laboratory analysis

At each station an acid-washed, 10 L plastic container was rinsed three times with surface water (0-2 m) from the underway water supply and then filled. The sample was given a unique identification number and the time at the start and at the end of the final water collection was noted. This was used together with the vessels navigation files to geolocate the sample. On one occasion where the vessels navigation recorder failed, we used hourly vessel positions to locate sampling.

Each 10 L container was mixed by inversion three times before subsamples were taken, processed and/or transported to the NIWA laboratory in Christchurch by overnight courier for further processing and laboratory analyses (Table 2-1):

- Total suspended matter (TSM): A 2 L subsample was placed in an acid washed plastic container and labeled for gravimetric analysis (Strickland & Parsons, 1972). A known volume was filtered onto a pre-weighed 25 mm diameter 0.7 um GF/F (glass fibre filter) and oven drying for total TSM, followed by combustion for the inorganic fraction (TSMi). Volatile, organic suspended matter (TSMo) was determined by difference.
- Coloured dissolved organic matter (CDOM): A 100 ml subsample was filtered through a pre-rinsed 25 mm diameter 0.2 um membrane filter into a pre-baked, labeled glass bottle and stored refrigerated prior to spectral absorption analysis following the method of Bricaud et al. (1981) for absorption a_{cdom} and slope S_{cdom} of exponential fit.
- Particulate absorption spectra (PABS): Subsamples (50 ml) of water were filtered through a 25mm 0.7 um GF/F until colour was uniformly visible on the filter (noting volume filtered and in subdued light to avoid pigment degradation). In clear oceanic water about 1 L was sufficient; much less was required in turbid water (about 150 ml). Once filtration was complete forceps were used to transfer the filter into a tissue-capsule. The capsule was then wrapped in a small square of aluminium foil and placed into liquid nitrogen. PABS scans were made on the filter before and after pigment extraction by methanol extraction and then bleaching following the method of Tassan & Ferrari (1995), to provide the total absorption by particles (a_p), the bleached remains, non-algal particles (a_{nap}) and by difference phytoplankton (a_{phy}).
- Pigments by high performance liquid chromatography (HPLC): The same procedure was followed as for PABS above but when filtration was finished, forceps were used to remove any visible zooplankton from the filter (as these contain pigments). The filter was folded in half, placed in a labelled cryovial and stored in liquid nitrogen. Pigments were extracted in 90% acetone by probe sonication and separated on a c8 column according to the method of Zapata (2000).
- Chlorophyll-a by fluorometry (ChlF): The same procedure was followed as for HPLC for duplicate filters, following the fluorometric method in Strickland & Parsons (1972).

Table 2-1: Summary of laboratory methods and parameters on surface water samples collected from the STB. See text for more information

Method	Full parameter name	Abbreviated parameter name	References	No. samples
ChlF	Surface concentration of chlorophyll-a (mg m^{-3})	Chl-a	Strickland & Parsons (1972)	52
HPLC	Phytoplankton pigment concentrations (mg m^{-3}), including chlorophyll-a	Chl-a, peri, diad, 19hex, 19but, (see Glossary for full names)	Zapata (2000)	52
SPM	Total suspended matter; organic fraction;inorganic fraction (mg m^{-3})	TSM, TSMo, TSMi	Strickland & Parsons (1972)	52
CDOM	Absorption by CDOM (m^{-1}); slope of the CDOM absorption curve (nm^{-1})	a_{cdom} (λ), S_{cdom}(λ)	Bricaud et al. (1981).	31
PABS	Absorption by phytoplankton and NAP (m^{-1})	a_p (λ),a_{phy} y(λ),a_{nap} t(λ)	Tassan & Ferrari (1995)	23

2.3 Specific inherent optical properties (sIOPs)

Collection sites broadly fall into two spatial areas, one around Wanganui in the north, and one in the south around Mana Island (Figure 1-1). Analysis of variance was performed on the specific inherent optical properties (sIOPs), which define optical water quality: a chlorophyll-specific absorption coefficient at 488 nm [a_{phy}(488)]; a sediment-specific absorption coefficient at 488 nm [a_{nap}(488)]; and the slope of the semi-logarithmic absorption curve of coloured dissolved organic substances (CDOM) - Table 2-2. In addition, ratios of two biomarker accessory pigments to chl-a were compared between the areas to assess whether the phytoplankton communities differed.

Apart from one pigment ratio, regions were not significantly different in all sIOPs, but hint at a difference in algal populations with significant differences in (Table 2-2). Both CDOM absorption at 412 nm and the slope of the semi-logarithmic CDOM absorption spectrum fall into a single distribution with a median value of $a_{cdom}(412) = 0.04$ m^{-1} and $S_{cdom} = 0.014$ nm^{-1}. No trends distinguishing the location groups were observed in the residuals.

The chlorophyll-specific concentrations of ancillary pigments fucoxanthin and 19' hexanoloxyfucoxanthin (hereafter 19hex) are not IOPs but provide insight into variability in the phytoplankton community composition. The absence of significant differences in the chl:fuco ratio suggests a comparable contribution of diatoms to the overall phytoplankton community. However, the difference in the chl:19hex ratio suggests different cell numbers, volumes or species of phytoplankton between the two areas. Further field measurements would be needed to determine the causes of spatial variability in phytoplankton assemblages, however, this is unlikely to affect the validity of the satellite data presented here.

Table 2-2: Specific inherent optical properties (sIOPs) models, chl-a specific pigment ratios and significance of differences between the northern and southern (Mana) STB areas (refer Figure 1-1).

Metric	sIOP model fit over all samples	No. samples to the north	No. samples to the south	Probability that samples are drawn from a single population
Chl-specific absorption	$a_{phy}(488) = 0.02826 chl.a + 0.00735$ $N = 22, r^2 = 0.22$	9	13	$P = 0.398$ (no statistical difference between regions)
Sediment-specific absorption	$a_{nap}(488) = 0.00789 TSMi + 0.00397$ $N=22, r^2= 0.56$	9	13	$P = 0.649$ (no statistical difference between regions)
Slope of CDOM absorption spectrum, S	$a_{nap}(\lambda) = a_{nap}(\lambda_0)\exp[S_{nap}(\lambda_0 - \lambda)]$ $N=21$ $a_{cdom}(412) = 0.040\ m^{-1}$ $S_{cdom} = 0.014\ m^{-1}$	13	8	$P = 0.689$ (no statistical difference between regions)
Chl-specific fuco	$fuco = 0.4454\ chl\text{-}a - 0.07118$; $N = 45, r^2 = 0.815$	18	27	$P << 0.010$ (significantly different populations)
Chl-specific 19hex	No significant relationship; $N = 45, r^2 = 0.037$	18	27	$P = 0.078$ (no statistical difference between regions)

2.4 Summary of *in situ* sampling data

The main parameters of interest are summarised for the summer and winter surveys as well as overall in Table 2-3. HPLC and fluorometric determinations of chl-a agreed well (R^2=0.62) with a small overestimation using the fluorometric method (data not shown). As recommended by NASA in protocols for satellite validation and calibration (Mueller et al., 2002), the subsequent analysis in this report is based on chl-a measured by HPLC. Chl-a concentrations measured in the STB ranged from 0.078 to 1.47 mg m^{-3} with a mean of 0.34 mg m^{-3}. Higher concentrations of chl-a were found during winter fieldwork in the STB.

Total suspended matter (TSM) concentrations ranged from 0.15–35 g m^{-3}, with a median value of 0.68 g m^{-3}. Only two *in situ* measurements of TSM were greater than 6 g m^{-3}, so the dataset is limited in its ability to validate satellite methods which estimate values greater than this concentration. The proportion of TSM which was organic was between 0.07 and 1, with a mean of 0.46, indicating high variability in the nature of the suspended matter but that a mineral (refractory) component is typically present in addition to organic (living and detrital) particulate material.

Absorption (at 412 nm) due to CDOM varied between 0.008 m^{-1} and 0.26 m^{-1}, with a mean of 0.076 m^{-1}. The high values indicate strong riverine sources of CDOM in some areas and at some times of the year.

Absorption by phytoplankton pigments, as indexed by $a_{phy}(488)$, was relatively constant throughout both measurement seasons with a mean of 0.017 ± 0.010 m^{-1}. However, the specific phytoplankton absorption, $a_{phy}(488)$/chl-a, increased from 1.85 ± 1.23 mg m^{-2} in summer to 22.0 ± 28.0 mg m^{-2} in winter, suggesting photo-adaptation to reduced light. The high variation in $a^*_{phy}(488)$ may be due to high concentrations of NAP in winter and low concentrations of chl-a, leading to elevated uncertainty in measurements of a_{phy}. Consequently, values of $a^*_{phy}(488)$ are not used to locally tune satellite processing in this report (see Section 3 for satellite processing methods).

Table 2-3: Summary of parameters collected in situ.

Parameter	All samples		Summer		Winter	
	Mean ± Std	N	Mean ± Std	N	Mean ± Std	N
TSM	2.0 ± 5.1	52	0.61 ± 0.51	26	3.4 ± 7.0	26
TSMo	0.27 ± 0.38	52	0.30 ± 0.13	26	0.49 ± 0.51	26
TSMi	0.41 ± 4.76	52	0.31 ± 0.41	26	2.89 ± 6.52	26
Chl-a	0.34 ± 0.25	52	0.27 ± 0.17	26	0.53 ± 0.24	26
$a_{cdom}(412)$	0.08 ± 0.06	31	0.06 ± 0.05	15	0.09 ± 0.07	16
S_{cdom}	0.014 ± 0.004	31	0.014 ± 0.005	15	0.013 ± 0.004	16
$a_{phy}(488)$	0.017 ± 0.010	23	0.021 ± 0.013	11	0.019 ± 0.007	12
$a^*_{phy}(488)$	3.0 ± 20.0	21	1.85 ± 1.23	12	22.0 ± 28.0	9

2.5 Phytoplankton communities

To determine if phytoplankton communities were different between summer and winter samplings, cluster analysis was applied to the concentrations of accessory pigments, normalised to HPLC-chl-a concentrations. No significant difference between the community compositions for winter and summer were found. However, clusters identified three distinctive pigment groupings (Figure 2-2). Class 1 was characterised by even contributions of 19'-hexanoyl-oxy-fucoxanthin (19hex), fucoxanthin (fuco) and peridinin (per). These are marker pigments for prymnesiophytes, diatoms and dinoflagellates, respectively (Jeffrey et al., 1997). Class 2 had elevated proportions of 19hex, the marker pigment for prymnesiophytes, and this phytoplankton taxon includes the calcifying coccolithophorid, *E. huxleyi*. Class 2 is of particular importance in remote sensing because calcifying coccolithophores exhibit extremely strong backscattering when calcite liths are shed at the end of a bloom (Balch et al., 1991). Class 3 featured low proportions of 19hex and higher fucoxanthin and peridin concentrations. The right panel in Figure 2-2 illustrates the phytoplankton community clusters discussed above. Although, no group was found exclusively in one spatial domain or season from our surveys, Class 3 (predominantly diatoms and dinoflagellates), was found in waters exceeding 30 m depth, whereas Classes 1 and 2 were also found in shallower waters.

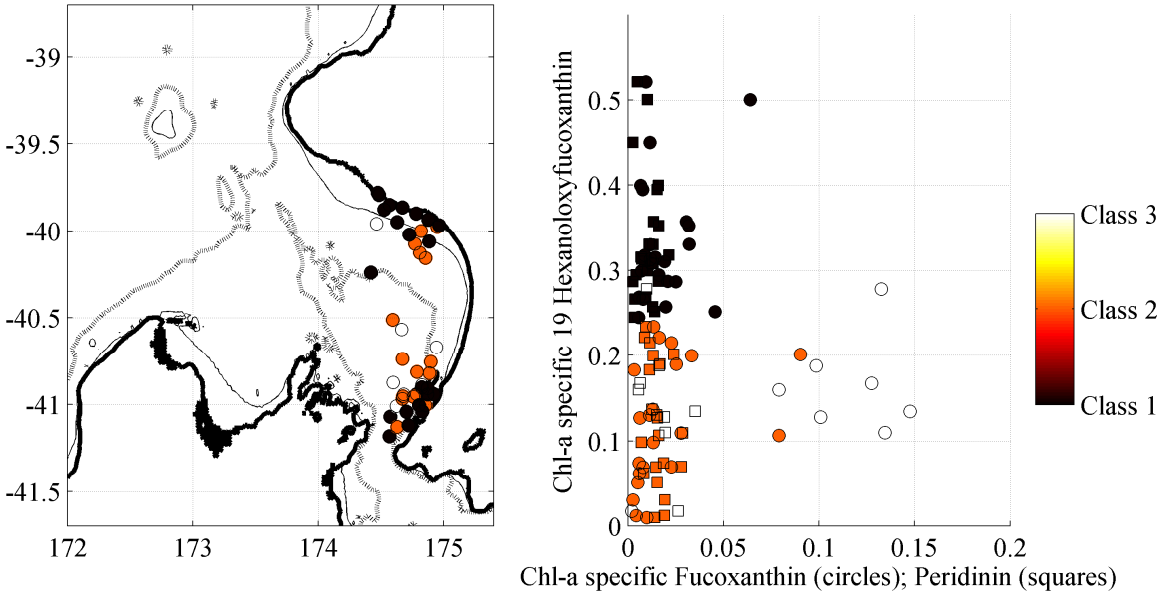

Figure 2-2: Left: *In situ* sample sites clustered according to their chlorophyll-specific proportions of marker pigments. Right: relative proportions of fucoxanthin (biomarker for diatoms), peridinin (biomarker for dinoflagellates) and 19'hexanoloxyfucoxanthin (biomarker for prymnesiophytes) within the three pigment clusters.

2.6 Covariance between chl-a, TSM, CDOM

High correlation between coloured material in the *in situ* data would limit our ability to use the data to locally tune ocean colour algorithms to the measurements. However, there is only weak co-variation between chl-a, TSM and absorption by CDOM (Figure 2-3a). The highest coefficient of determination, for the chl-a vs TSM relationship (R^2=0.53) is driven by the single high data point (TSM = 35.5 g m^{-3}). Without this point (Figure 2-3b), R^2 is much smaller (0.28). The relationships between chl-a and CDOM absorption (Figure 2-3c) and between TSM and CDOM absorption (Figure 2-3d) are weak (R^2 of 0.23 and 0.04 respectively).

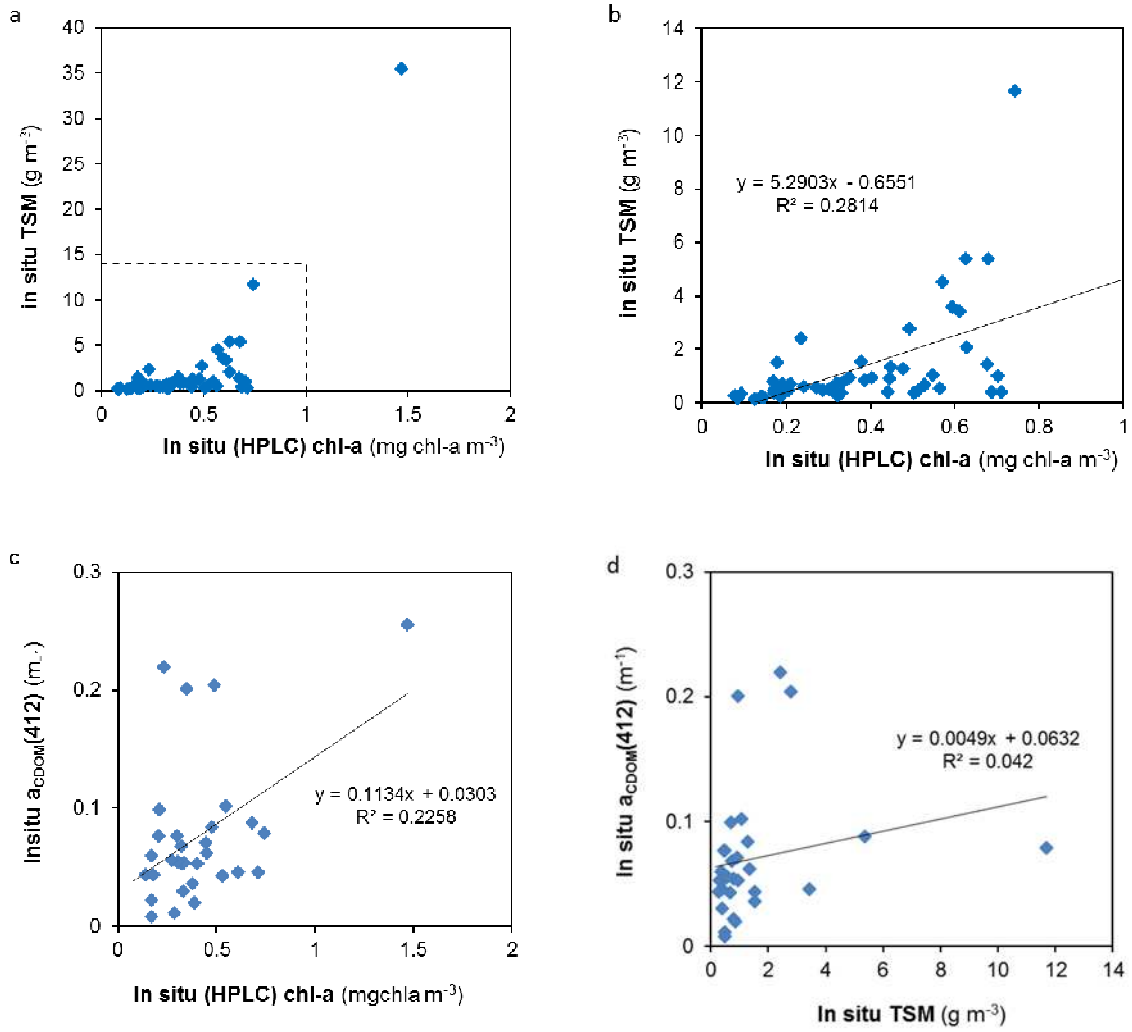

Figure 2-3: Covariance between *in situ* measurements of chl-a concentration (by HPLC), gravimetric total suspended matter concentration measured from filtered water samples (TSM), and absorption by coloured dissolved organic matter (CDOM). Note that (b) shows the same data as (a) within the dashed lines only. Generally, there is low covariance between the data.

3 Satellite products, algorithms and processing

3.1 Source of satellite data

All ocean colour satellite data used in this report are from the Moderate Resolution Imaging Spectrometer (MODIS), on the Aqua satellite, owned and operated by the US National Aeronautics and Space Administration (NASA). Level 1A (top of atmosphere, calibrated) MODIS-Aqua imagery was acquired from the Ocean Biology Processing Group at NASA, for the STB area from 172° to 175.4° E; and 38.7° S to 41.7° S.

Ocean colour remote sensing of turbid, coastal waters is an evolving field of research internationally, with many approaches proposed by different researchers. At present, no approach has been demonstrated to be more appropriate than others in the STB.

In this study we considered a selection of the processing methods available within the current version of the ocean colour processing software SeaDAS v6.5.7. There are two parts to the data processing of ocean colour data: (1) atmospheric correction to obtain the spectrum of water leaving radiance; (2) in-water algorithm to estimate IOPs and/or concentrations of water constituents. For the purposes of this report, we chose those processing methods most likely to deliver useful results and evaluated these against the *in situ* measurements in the STB. The processing methods considered were exclusively those selected by and supported by NASA within the SeaDAS processing software. We acknowledge that there are a large number of atmospheric correction and in-water algorithms which we did not consider (e.g. Garver & Siegel, 1997; Ruddick et al., 2000; Lavender et al., 2005; Pinkerton et al., 2006; Doerffer & Schiller , 2007; Shanmugan, 2011). Nevertheless, focussing on the key set of NASA-supported approaches is likely to provide the most robust result. It is likely that algorithms for remote sensing of coastal waters will continue to develop, and it may be worthwhile to revisit the selection of the most promising methods in the future.

All parameters were calculated at a pseudo-spatial resolution of 500 x 500 m, using one MODIS band with 250 x 250 m resolution, one with 500 x 500 m resolution and the remaining colour bands at 1000 x 1000 m resolution.

3.2 Atmospheric correction

Atmospheric correction was applied using the NIR/SWIR switching algorithm (Wang & Shi, 2007). Although there are alternative approaches to atmospheric correction over turbid waters (e.g. Ruddick et al., 2000; Lavender et al., 2005), the NIR/SWIR approach is the version chosen by NASA for support and is the most widely-used approach internationally. A pixel-by-pixel approach to atmospheric correction (such as the NIR/SWIR approach) was preferred over a scene-based approach to atmospheric correction in order to capture small-scale variability in aerosols near-shore. Validating atmospheric correction of ocean colour over turbid coastal waters in a dynamic and highly cloudy region such as the STB is a scientifically-challenging, expensive and long-term undertaking. It was hence not possible to validate the MODIS atmospheric correction scheme within the constraints of this study.

3.3 In-water algorithms

Three products are required from the in-water algorithms: chlorophyll-a concentration, total suspended matter concentration, and absorption by CDOM. We used the Quasi-Analytical

Algorithm (QAA update v5: Lee et al., 2002; Lee et al., 2009) to derive these. The MODIS QAA algorithm takes the spectrum of remote sensing reflectance as input and uses a combination of empirical relationships and radiative transfer theory to estimate absorption by phytoplankton, absorption by detrital material (both particulate and dissolved) and total particulate backscattering at each input wavelength. For example, the QAA algorithm uses an empirical relationship to estimate absorption at 555 nm from reflectance in red, green and blue bands. This, and other empirical relationships within the QAA algorithm, were developed from large "global" datasets and represent "average" or "typical" relationships between bio-optical parameters occurring in natural coastal and marine waters.

For semi-analytical in-water algorithms like QAA it is possible to compare each of the key relationships used in the algorithm against local measurements and potentially adjust these relationships to better represent local conditions. However, our ability to locally tune the QAA algorithm in this STB was limited by two factors. First, the set of measurements it was possible to take within this project was limited and included no *in situ* radiometric measurements or *in situ* measurements of backscattering. Second, the number of data points is low (~50) and coverage of the domain in time and space was limited. Consequently, it was not reasonable to use the *in situ* data to adjust the empirical relationships within the QAA algorithm.

The QAA algorithm estimates three key IOPs, namely: (1) absorption of phytoplankton at 488 nm (APH488); particulate backscattering at 488 nm (BBP488); and total (i.e. particulate and dissolved) detrital absorption at 412 nm (ADET412). These IOPs must then be converted to the biogeochemical properties of interest, namely chl-a concentration, TSM concentration and CDOM absorption. The appropriate conversion to use for these conversions are highly region specific. These conversion factors were derived from *in situ* measurements in the STB as part of sampling funded by TTR as described below.

3.3.1 Alternative algorithms for chl-a concentration

We chose not to use the MODIS Case 1 (open ocean) band-ratio algorithm for chl-a (O'Reilly et al., 1998) because this method of processing is not valid where suspended sediment and/or CDOM from terringinous sources (riverine run-off, resuspension of bottom sediments or material from coastal erosion) are present. In turbid coastal waters, the suspended particulate material leads to chl-a concentrations being overestimated. We tested the performance of this algorithm in the STB and confirmed this erroneous behaviour when moderate and high concentrations of TSM (>1 g m^{-3}) were present (data not shown).

An alternative to semi-analytical algorithms for chl-a in coastal waters is the MODIS normalised fluorescence line height product (FLH: Letelier & Abbott, 1996). Chl-a fluoresces in the red (around 683 nm) and the height of the solar-stimulated fluorescence emission line is related to the concentration of chl-a in the water (Letelier & Abbott, 1996). The MODIS FLH product is hence potentially useful for estimating chl-a concentration in turbid waters because it is unlikely to be affected by co-occurring sediment (Hu et al. 2005; McKibbon et al. 2012). Also, the FLH product is not affected by CDOM loading (Hoge et al., 2003). However, the relationship between fluorescence and chl-a concentration depends somewhat on the physiological state of the phytoplankton community, including, the rate of photosynthesis and whether nutrients or light availability are limiting productivity (Letelier & Abbott, 1996). The relationship between FLH and chl-a concentration can also be affected by

the intensity of the incident light and phytoplankton functional group (e.g. diatoms, dionoflagellates etc). In other areas of New Zealand, these factors mean that FLH provides poor estimation of chl-a concentration in coastal waters over long time periods (more than a few days) (Pinkerton, unpublished data). Because of this, and the fact that we do not have sufficient information to attempt to correct for these changes in across the study area, we did not use the MODIS FLH product to estimate chl-a concentration in this study.

3.3.2 Alternative algorithms for TSM concentration

There were two alternative candidate satellite products available from which to estimate TSM concentration: band-ratio TSM (Clark, 1997) and the MODIS PIC (particulate inorganic carbon) algorithm (Balch, 2010).

The Clark (1997) band-ratio TSM algorithm estimates a generic or "global average" concentration of TSM. It was developed by empirical fitting to a reasonably-large "global" dataset of the relationship between spectral water reflectance and TSM concentrations. The optical properties of naturally-occurring TSM vary considerably around the world as a consequence of variations in properties such as sediment size distribution, refractive index, particle shapes, and attached organic matter. Hence, the Clark band-ratio estimates must be locally tuned to estimate TSM concentration occurring in the STB. Although it is possible to derive a correction based on end-to-end "match-ups" between MODIS-derived TSM and in situ measurements, the robustness of this correction is difficult to ascertain and we did not use this product.

The MODIS PIC algorithm was developed to estimate the concentration of detached coccolithophore plates in oceanic waters and hence estimates a parameter (molC m^{-3}) that is related to TSM concentration in an ill-defined manner. For example, it is not known whether the relationship between PIC and TSM should be linear or non-linear, and we have no data to test for departure from linearity at high TSM concentrations. Consequently, we do not use this product.

3.3.3 Alternative algorithms for CDOM absorption

The only available alternative method of estimating CDOM was the MODIS CDOM_index product (Morel & Gentili, 2009). The CDOM_index is the ratio by which the CDOM absorption exceeds that expected in Case 1 (oceanic) waters based on the estimated chl-a concentration (Morel & Gentili, 2009). In coastal waters with input of CDOM from riverine run-off, the CDOM_index would always be expected to exceed 1, potentially by large amounts. However, overestimates of chl-a in the coastal zone because of suspended sediment being misidentified as chl-a by the standard MODIS band ratio algorithm would lead to values of the CDOM_index that are too low (and less than 1). As such, the CDOM_index product is poorly suited for use in turbid coastal waters and was not used in this study.

3.3.4 Conversion factors for the QAA algorithm

Three factors were used to convert IOPs (as estimated by the QAA processing) to the required parameters for the STB:

(1) **chl-a specific absorption at 488 nm** [a_{ph}*(488)] was used to convert absorption of phytoplankton at 488 nm (APH488) to chl-a concentration. Phytoplankton specific absorption typically decreases with increasing absorption by phytoplankton as a result partially of the

'package effect': as the concentration of phytoplankton increases, the proportion of the pigment which interacts with a light beam decreases because of self-shading (Bricaud et al. 1995; Bissett et al. 1997). Consequently, a non-linear dependence of chl-a on absorption by phytoplankton is likely. We used the parameterisation of Bricaud et al. (1995) for $a_{ph}^*(\lambda)$ as equation 1 where $A(488)=0.0279$ and $B(488)=0.369$. Measurements of phytoplankton absorption in the STB agree well with the Bricaud et al. (1995) parameterisation (Figure 3-1) and no local adjustment is warranted.

$$a_{ph}^*(\lambda) = A(\lambda)chl^{-B(\lambda)} \qquad \text{[equation 1]}$$

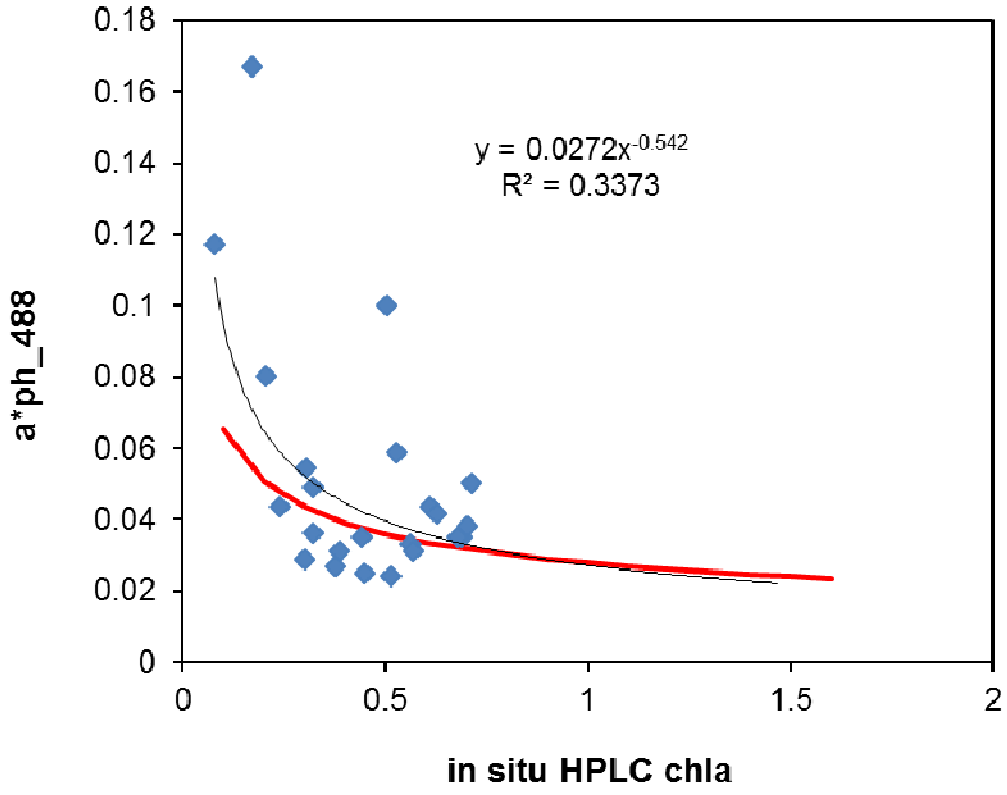

Figure 3-1: Chlorophyll-a specific absorption at 488 nm. Chlorophyll-a specific absorption by phytoplankton at 488 nm (a*ph_488) measured in situ in South Taranaki Bight (blue diamonds). Least squares fitted power-law regression line (black, equation shown) and relationship from Bricaud et al. (1995) (red line).

(2) **TSM-specific backscattering at 488 nm** [$b_b^*(488)$] was used to convert particulate backscattering at 488 nm (BBP488) to TSM concentration. Note that TSM includes both phytoplankton and NAP material. No *in situ* measurements of baskscattering were available in the STB but samples of sediment were brought back for subsequent laboratory analysis (Gall et al., 2013). Backscattering (and other IOPs) of a given mineralogy of particulates vary substantially depending on the wavelength of light and the size of the particle (indexed by a

nominal particle diameter, *D*). As described in Gall et al. (2013), sediment samples collected from the STB were brought back to the Wellington NIWA optical laboratory, separated into five size classes by settling, and the specific backscattering coefficients measured using the ECO-VSF3 meter (Wetlabs Inc.). Based on these measurements, optical modelling was used to estimate $b_b^*(\lambda)$ as a function of *D*. Not surprisingly, there was substantial variation in $b_b^*(488)$ with particle size – more than a factor of 600 variation between *D*=0.1 and 100 μm. The appropriate value of $b_b^*(488)$ is hence highly dependent on the particle size distribution (PSD) of naturally occurring sediment in the upper water column of the STB.

We used PSD measured in the STB and reported in MacDonald et al., (2013, figures 3.13, 3.29b, 3.29c). These PSDs give values of $b_b^*(488)$ between 0.0051 and 0.014 $m^2\ g^{-1}$, equivalent to *D* between 11.1 and 24.5 μm. Here we used a mean PSD to estimate $b_b^*(488)$=0.0088 $m^2\ g^{-1}$ (equivalent to *D*=17 μm) which was used to convert the QAA BBP488 product to TSM.

More information on the appropriate PSD for naturally occurring sediment in the STB is given by comparing data on the beam attenuation at 530 nm measured in the STB (MacDonald et al. 2013, figures 2.3 and 2.4). The TSM-specific beam attenuation at 530 nm, [$c^*(530)$] based on these measurements was 0.211 $m^2\ g^{-1}$. Size-specific measurements of c*(530) from tank experiments (Gall et al., 2013) implies this is equivalent to *D* of 22.9 μm, within the range estimated above based on figures 3.13 and 3.29b/c (MacDonald et al., 2013).

PSD will vary across the STB in time and space, depending on proximity to different sources of sediment, levels of turbulence and mixing, and differential settling of particles of different sizes. Hence, the use of a single value of $b_b^*(488)$ for all pixels in all satellite images (i.e. all locations and all times) will lead to errors in estimated TSM concentrations, even if the satellite-derived estimates of $b_b^*(488)$ were exact. Sediment closer to the shore is likely to have larger particles while material offshore is likely to be finer. This spatial variation in the particle size spectrum of naturally-occurring material means that TSM is likely to be underestimated close to the shore and overestimated offshore. The level of uncertainty caused by this effect is estimated to be of the order of -40% to +60% (i.e. underestimates of 40% or overestimates of 60% are possible because of variation in PSD in time and space). This uncertainty is small compared to the variation in the long-term median TSM concentration derived from the 11-years of satellite data. The median TSM varies by a factor of 170 across the STB, from 0.17 g m^{-3} to 29 g m^{-3} (see later in this report). The day-to-day variation in TSM seen from image to image will be much greater than this.

(3) **NAP-specific absorption at 412 nm** [$a_{nap}^*(412)$] was used to correct total (i.e. particulate and dissolved) detrital absorption at 412 nm (ADET412) for the absorption due to NAP to estimate CDOM absorption. Note that ADET412 does not include the absorption due to phytoplankton, and so no correction for phytoplankton-specific absorption is required. TSM-specific absorption at 412 nm was measured in the NIWA Wellington optical laboratory based on samples from the STB, and was found to be $a_{nap}^*(412)$=0.0332 $m^2\ g^{-1}$ (Figure 3-2).

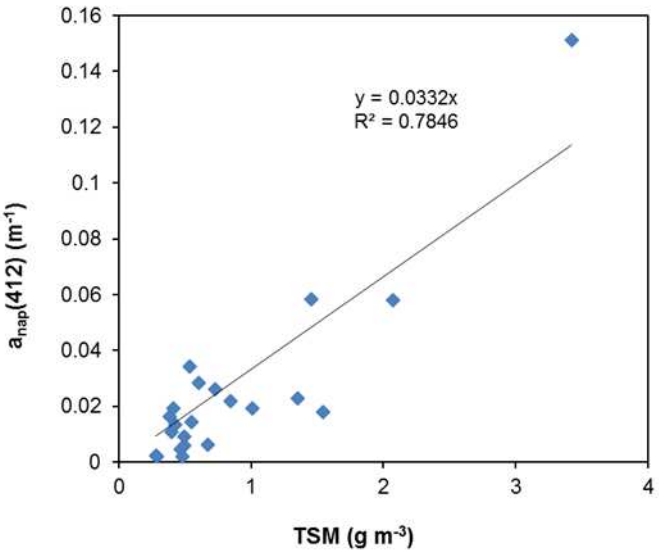

Figure 3-2: *In situ* measurements of absorption by non-algal particles (nap). Non-algal particle absorption was measured in the laboratory by spectrophotometry after bleaching and is plotted against total suspended matter concentration (TSM). The value of a_{nap}*(412)=0.0332 m^2 g^{-1} was used to correct the ADET412 product from the MODIS QAA algorithm for NAP absorption and hence estimate CDOM absorption.

3.4 Local validation by match-up analysis

"End-to-end comparison" or "match-up" approaches can be used to test how well satellite data corresponds to *in situ* measurements of water properties. In this approach, ideally, satellite data products are compared to *in situ* measurements of the same property at the same location and at the same time (a "match-up"). This method can hence provide validation of the entire satellite data processing method, including calibration of the satellite sensor, atmospheric correction methods, satellite geolocation accuracy and in-water algorithm performance. However, in reality, there are three main problems with this approach. First, the spatial scale of the *in situ* sampling is much smaller than that of the satellite sampling (a few ml of water compared to an area of some 250,000 m^2 of ocean surface (the area of one 500 m pixel). Variability in water constituents will lead to differences in the end-to-end comparison even if the satellite observation method was perfect. Second, as each location is observed by satellite only once or twice daily, sampling by boat can give only this number of exact match-ups in time and space (and even this is very hard to achieve in practice) and so a large number of ship-days is needed to build up a validation dataset of reasonable size. Third, a match-up is obtained only if the *in situ* sampling occurs where there is no cloud. In very cloudy regions (such as the STB), sampling over long periods (many months at least) would be required. One way of addressing issue (2) is to compare average satellite data within a few pixels of the *in situ* sampling location. Here, we used a mean of 9 pixels. The usual way of addressing issue (3) is to compare satellite data taken within a few hours or even days of the *in situ* sampling.

In this study, each of the candidate products was extracted from each image covering the period of the biogeo-optical fieldwork (2011 day 335 to year 2012 day 213), and matched to the *in situ* data where possible. Because of cloud cover, there were too few match-ups on the exact day for useful comparisons. Hence, for each of the 52 *in situ* biogeo-optical stations we extracted data at the location of the *in situ* sampling from the three satellite overpasses that are closest in time to the sampling. The data were only used for calibration/validation of the satellite data if two conditions were met:

1. the mean time difference between the *in situ* sampling and the 3 closest satellite overpasses with valid data at that point was less than 10 days.
2. the coefficient of variation (CV), defined as the ratio of the standard deviation to the mean of the 3 extracted data points, was less than 1.

The requirement for this approach to be useful is that the change in water properties between *in situ* and satellite measurement must be less than the variability in water properties in the study domain in general. The uncertainty caused by this time difference was tested as follows. Consider the time series of a water property (e.g. chl-a concentration) observed at a given point by satellite over the 10-year satellite record. Pick one observation of this property (denoted x), pretend this is an *in situ* observation and apply the rules above to derive the satellite match-up value that would be obtained (denoted y). Note that in many cases no valid match-up value y would be derived at all. Because satellite observations of a given location may occur in groups in time (e.g. because low cloud weather patterns last a few days), match-ups were also excluded where the mean time difference between the (pseudo) *in situ* sampling and satellite observation was too low (less than the minimum in the real data set of 0.68 days). When a valid match-up value y is obtained, the log ratio is estimated as $\varepsilon=\ln(y/x)$. The mean value of ε calculated over all valid match-ups at a given point gives an estimate of the bias caused by this method of comparison. The mean value of the absolute (or alternatively squared) value of ε calculated over all valid match-ups at a given point gives an estimate of the uncertainty in the comparison caused by variability in the water over the time difference between *in situ* sampling and satellite observation. This analysis suggests that uncertainties are of the order of factors of between 2 and 4. This match-up analysis should be recognised as giving only order-of-magnitude validation.

Comparisons of satellite-derived and *in situ* measurements are given below for chl-a concentration (Figure 3-3), TSM concentration (Figure 3-4) and absorption by CDOM at 412 nm (Figure 3-5). For chl-a, the satellite data explains 38% of the deviance in the *in situ* measurements and the magnitudes of the estimates are similar. The comparison suggests that the satellite data may underestimate chl-a. About 48% of the deviance in field measurements of TSM concentration is explained by the satellite observations according to the end-to-end comparison, with little evidence of a substantial over- or under-estimate. It is noted that the TSM concentrations available for this analysis are relatively low compared to concentrations likely very close to the coast in the STB. For CDOM, only 15 comparisons were possible, but 56% of the variance in *in situ* measurements of CDOM absorption was explained by the satellite observations. Overall, these match-up analyses give good confidence that the satellite data presented in this study are fit for purpose.

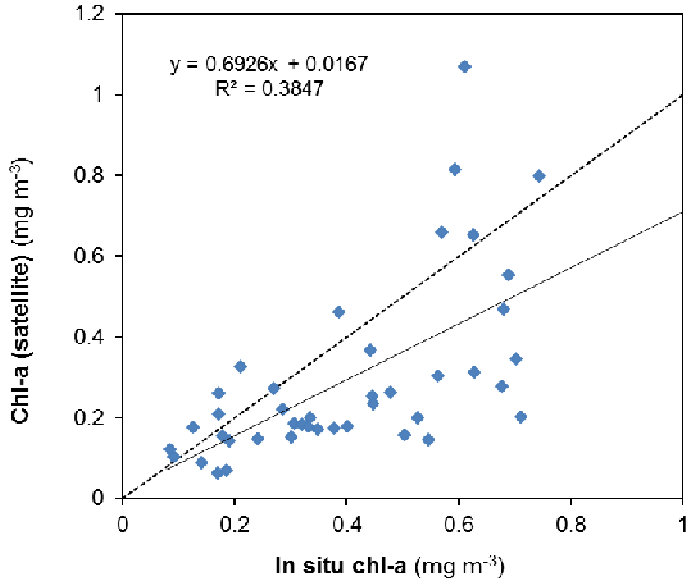

Figure 3-3: End-to-end validation of chlorophyll-a (chl-a) concentration. *In situ* measurements were compared to observations by satellite taken as close as possible in time and space (as described in the text). This method of comparison is useful for only order of magnitude validation. Solid line and equation is the least-squares regression. The dashed line shows 1:1 correspondence.

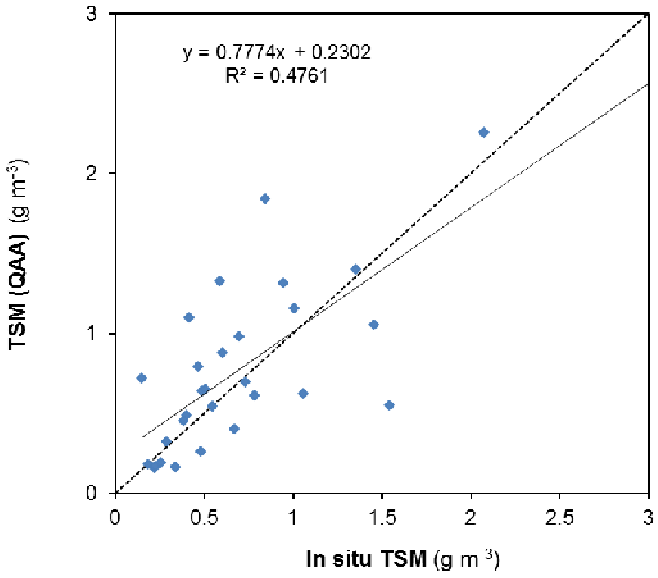

Figure 3-4: End-to-end validation of total suspended matter (TSM) concentration. *In situ* measurements were compared to observations by satellite taken as close as possible in time and space (as described in the text). This method of comparison is useful for only order of magnitude

validation. Solid line and equation is the least-squares regression. The dashed line shows 1:1 correspondence.

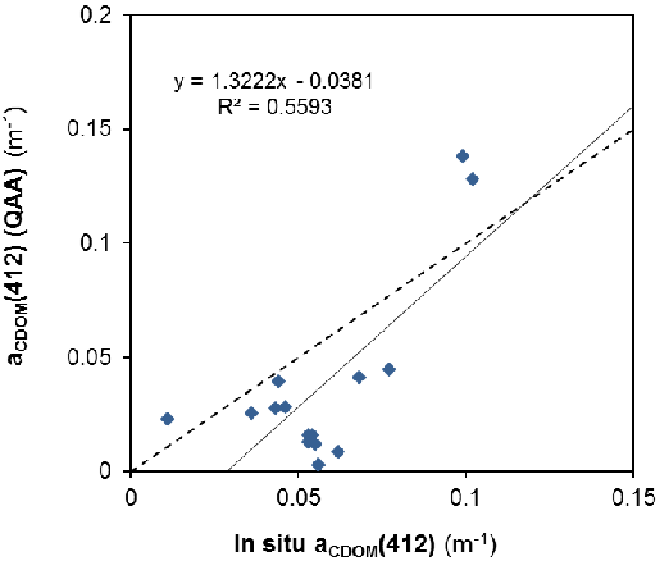

Figure 3-5: End-to-end validation of absorption by coloured dissolved organic matter (CDOM) at 412 nm. *In situ* measurements were compared to observations by satellite taken as close as possible in time and space (as described in the text). This method of comparison is useful for only order of magnitude validation. Solid line and equation is the least-squares regression. The dashed line shows 1:1 correspondence.

3.5 Summary of satellite processing used in this study

- Atmospheric correction was applied using the NIR/SWIR switching algorithm (Wang & Shi, 2007), which performs pixel-by-pixel correction and is valid in turbid waters. No local tuning or validation of the atmospheric correction procedure alone was possible.
- Water reflectance spectra were converted to three key IOPs using the Quasi-Analytical Algorithm (QAA update v5: Lee et al., 2002; Lee et al., 2009). No local tuning or validation of the QAA algorithm alone was possible.
- Chl-a concentration was obtained from a scaling of the absorption of phytoplankton at 488 nm (QAA product APH488). Conversion factors from Bricaud et al. (1995) were used and these were successfully validated against local measurements in the STB.
- TSM was obtained from a scaling of particulate backscattering at 488 nm (QAA product BBP488). The conversion factor used was derived from local measurements of backscattering by non-algal particles in the STB region.
- Absorption by CDOM at 412 nm was estimated by correcting the total (i.e. particulate and dissolved) detrital absorption at 412 nm (QAA product ADET412) for absorption

due to NAP alone. The correction factor was derived from measurements of NAP absorption in the STB region.

- End-to-end comparisons between in situ observations of chl-a concentration, TSM concentration and absorption by CDOM give good order-of-magnitude validation and give good confidence that the satellite data presented in this study are fit for purpose.

3.6 Extraction of satellite data

Five sites in the STB were chosen for time series analysis to illustrate the natural background variation in TSM, chl-a, and detrital absorption over the history of available satellite data. Three sites were located over the inner (I), mid (M), and outer (O) parts of the proposed mining region (Figure 1-1 and Table 3-1). A further three sites were located within 10 km of the shore towards the north (N), south (S) and off the Whanganui River (W) (Figure 1-1 and Table 3-1). Additionally, in recognition of the likely differences in water constituents with distance from the coast, we also defined four zones based on distance offshore from the coastline, up to 40 km (Figure 3-6).

Table 3-1: Locations for time-series analysis of satellite data at specific locations (Figure 1-1) and for specific zones Figure 3-6).

Locality	Latitude	Longitude
Inner end of mining area (A)	39.850° S	174.194° E
Outer end of mining area (B)	39.888° S	174.070° E
Indicative northern site “North” (N)	39.750° S	174.200° E
Near Whanganui river mouth (W)	40.050° S	174.850° E
Indicative northern site “South” (S)	40.500° S	175.100° E
0–10 km from coast	39.2° – 40.8° S	173.4° – 175.2° E
10–20 km from coast	39.2° – 40.8° S	173.4° – 175.2° E
20–30 km from coast	39.2° – 40.8° S	173.4° – 175.2° E
30–40km from coast	39.2° – 40.8° S	173.4° – 175.2° E

a

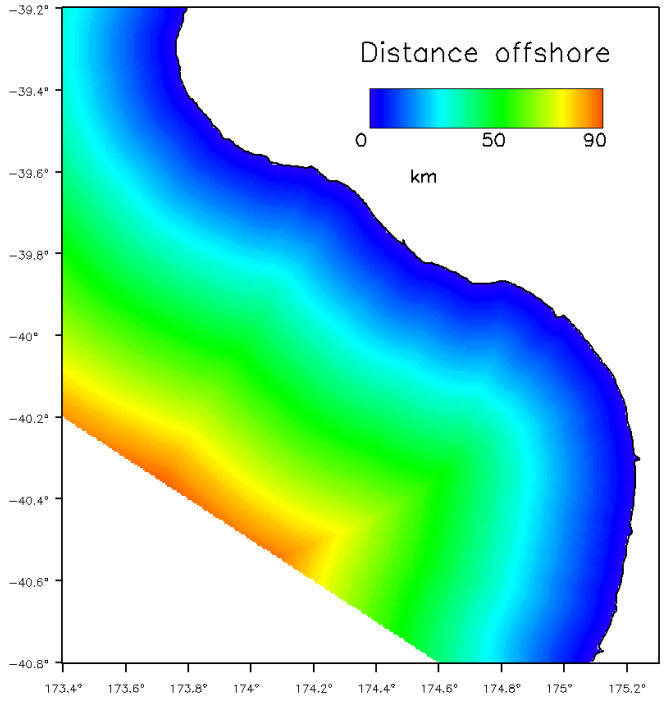

b

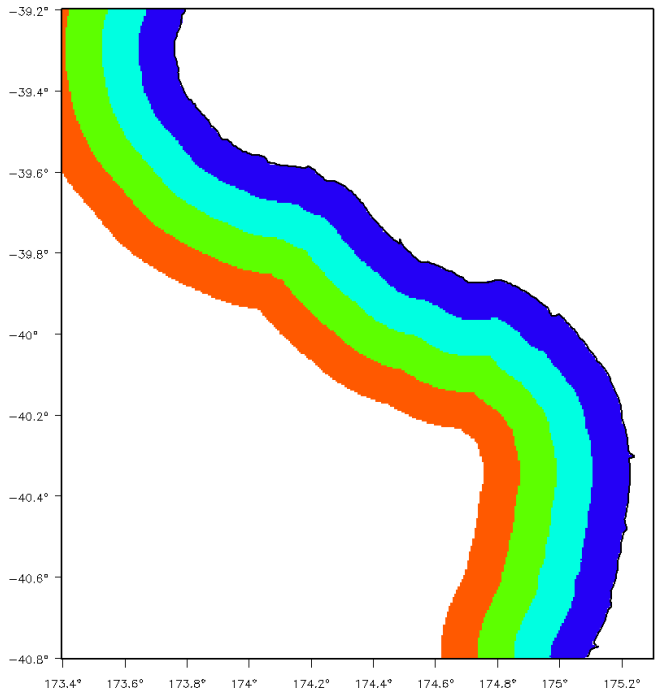

Figure 3-6: a: Distance offshore in the study area (km); b: Four bands representing different distances offshore for summarizing onshore-offshore trends in satellite data: 0-10 km (blue); 10-20 km (cyan); 20-30 km (green); 30-40 km (red).

4 Objective 3: Satellite total suspended matter (TSM)

4.1 TSM concentration

Averaged over the entire MODIS data 10 year record (2002-2012), TSM was distributed through the STB as shown in Figure 4-1. Monthly climatologies are shown in Figure 4-2, and mean values are shown in Figure 4-3. Three obvious zones appear in these maps: (1) a near shore area with high TSM (within about 5 km of the coastline, median ~2 g m^{-3}, interquartile range 0.5–5.5 g m^{-3}, 95th percentile of 18 g m^{-3}); (2) a transition zone with medium concentrations from about 5 to 10–15 km offshore, median 0.4 g m^{-3}, interquartile range 0.1–0.7 g m^{-3}, 95th percentile of 2 g m^{-3}); and (3) a low concentration offshore area (>15–20 km offshore, median of 0.2 g m^{3}). The highest TSM concentration observed in the satellite data was 81 g m^{3}.

TSM concentrations in the satellite dataset were highest in July, decreasing to a minimum monthly average in February. Figure 4-4 shows the extracted ten-year time-series of satellite-derived TSM at two mining sites (inner and outer) labeled A and B respectively in Figure 1-1. Similarly, Figure 4-5 shows the ten-year time-series of satellite-derived TSM at the three coastal sites located to the north, south and centrally at the Wanganui River mouth (labeled N, W, S in Figure 1-1). Satellite coverage was lower at coastal sites W and S, and the seasonal pattern was less consistent. This reflects the sporadic occurrence of high-sediment conditions related to increased river flow events. The statistical distribution of TSM at each site is summarized in Figure 4-6. Over the past ten years, there has been no temporal trend in TSM concentrations at any of the selected sites ($p > 0.01$).

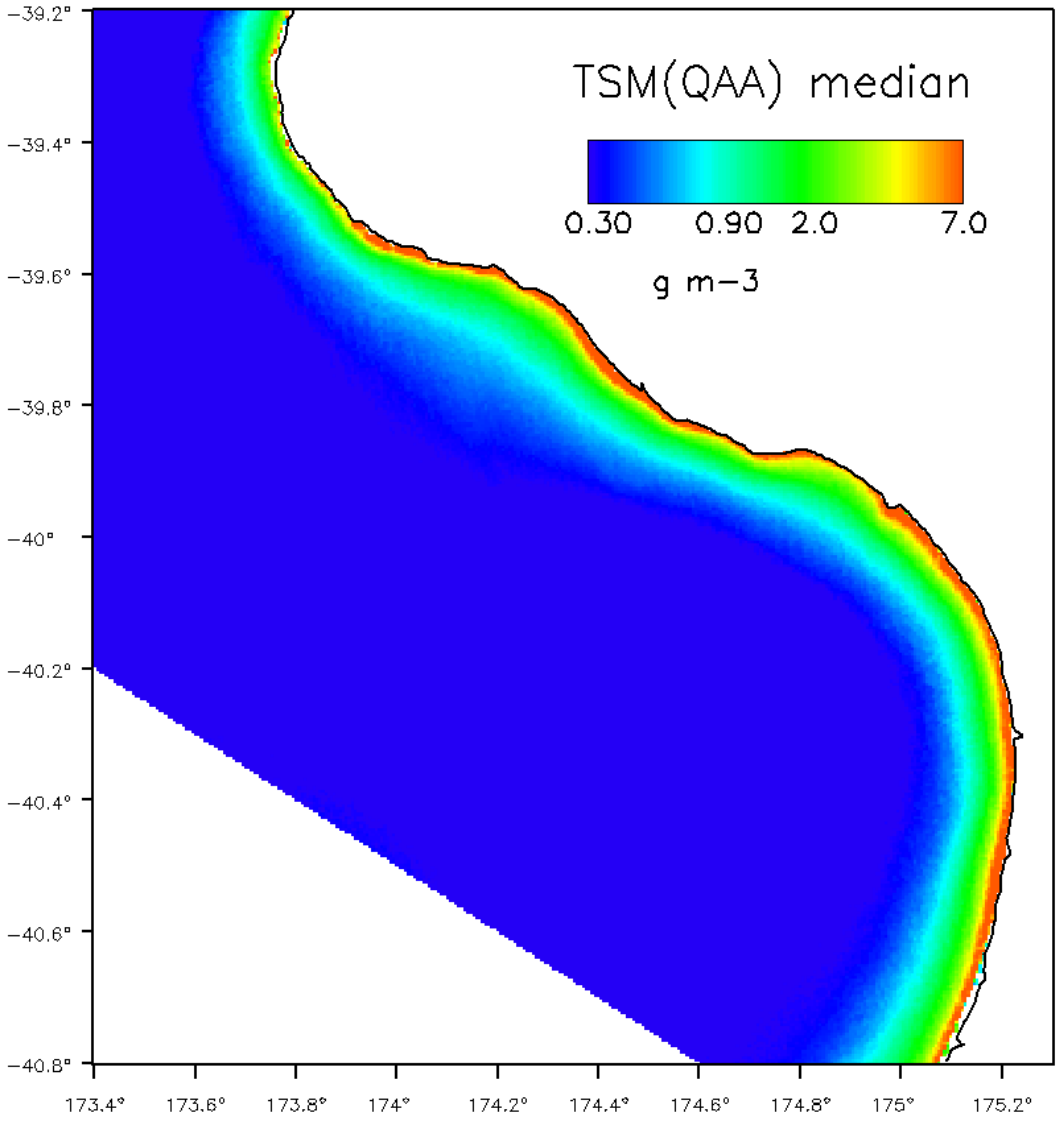

Figure 4-1: Spatial distribution of the long-term mean total suspended matter (TSM) based on particulate backscatter at 488 nm from the QAA algorithm. Values were calculated as the median value over ten years of MODIS-Aqua data in each pixel. Note the logarithmic scale in concentration.

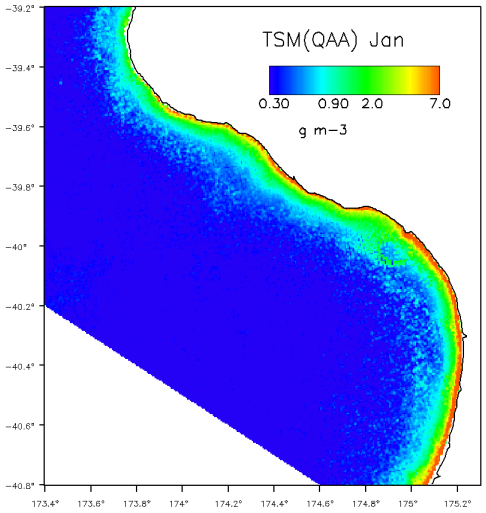
TSM(QAA) Jan
0.30 0.90 2.0 7.0
g m−3

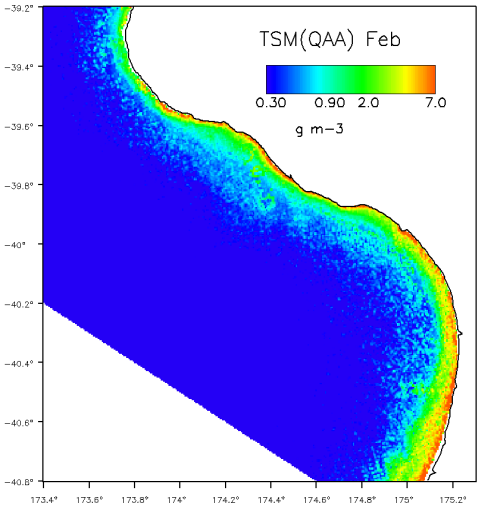
TSM(QAA) Feb
0.30 0.90 2.0 7.0
g m−3

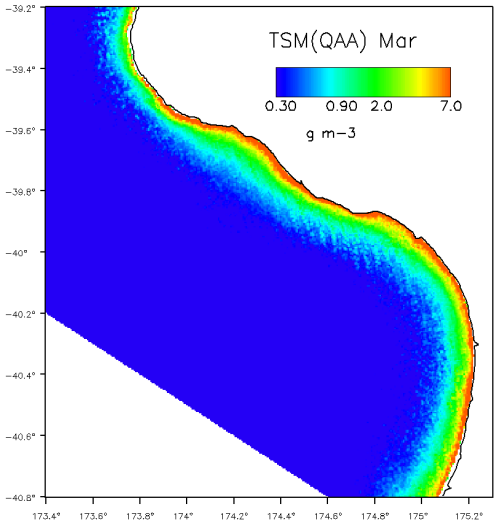
TSM(QAA) Mar
0.30 0.90 2.0 7.0
g m−3

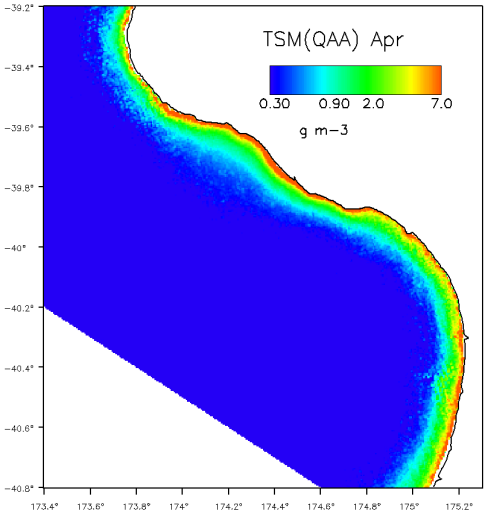
TSM(QAA) Apr
0.30 0.90 2.0 7.0
g m−3

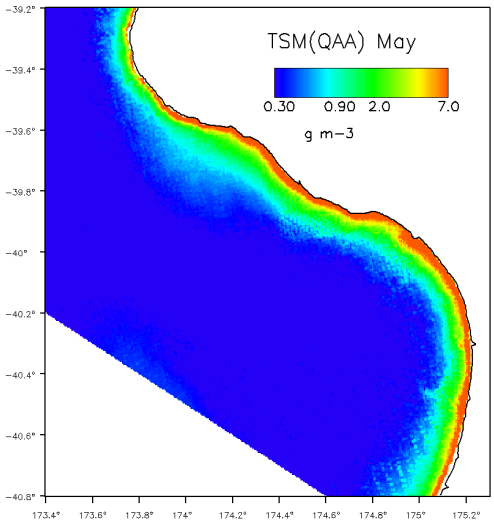
TSM(QAA) May
0.30 0.90 2.0 7.0
g m−3

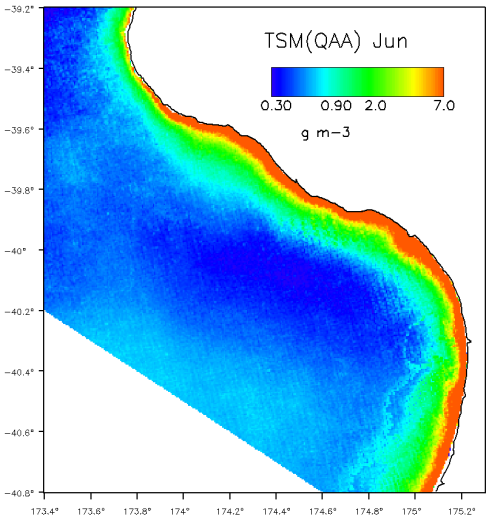
TSM(QAA) Jun
0.30 0.90 2.0 7.0
g m−3

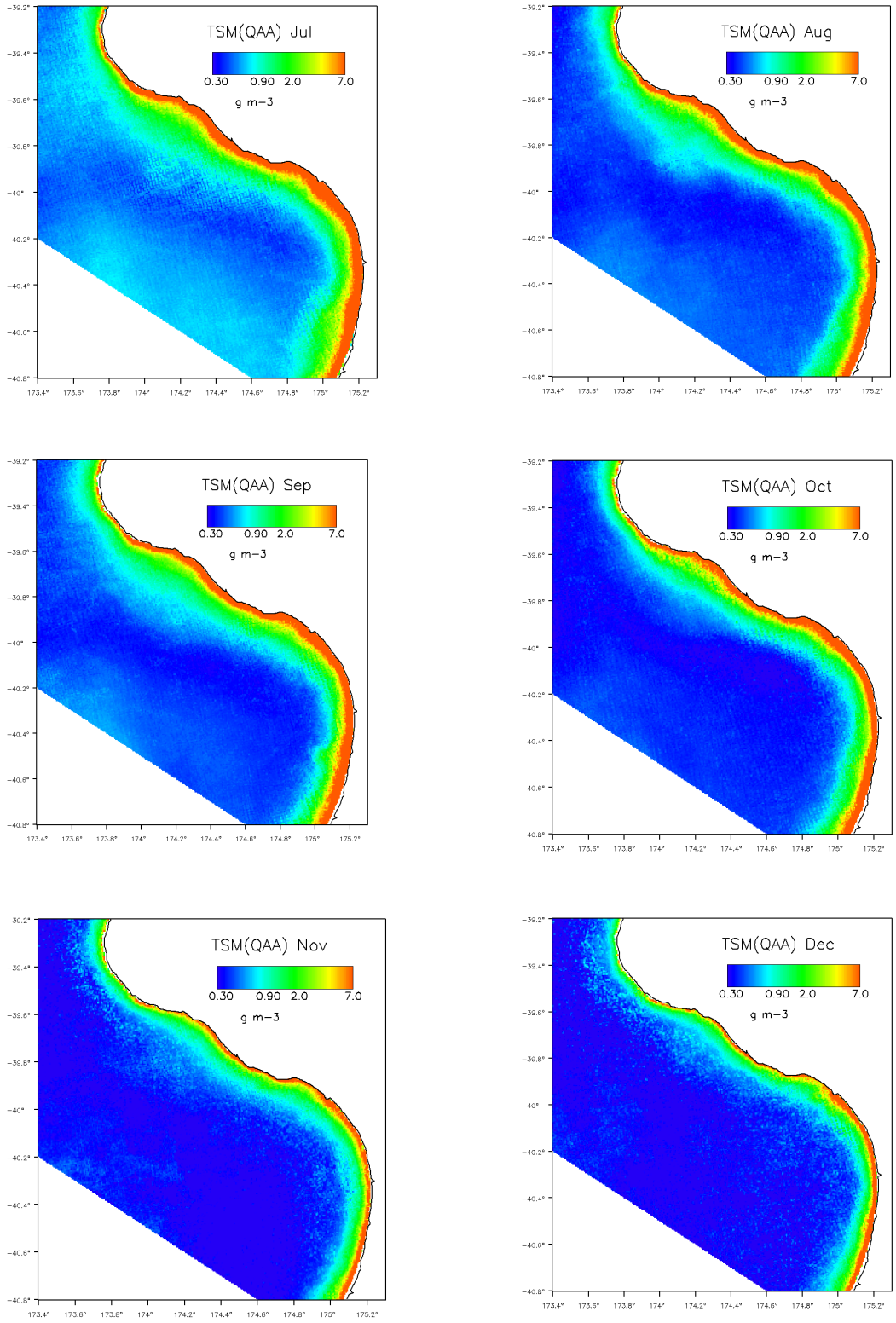

Figure 4-2: Monthly climatology of total suspended matter (TSM) based on particulate backscatter at 488 nm from the QAA algorithm. Monthly averages were calculated over ten years of MODIS-Aqua data. Colour scales are logarithmic and are the same in each plot and in Figure 4-1.

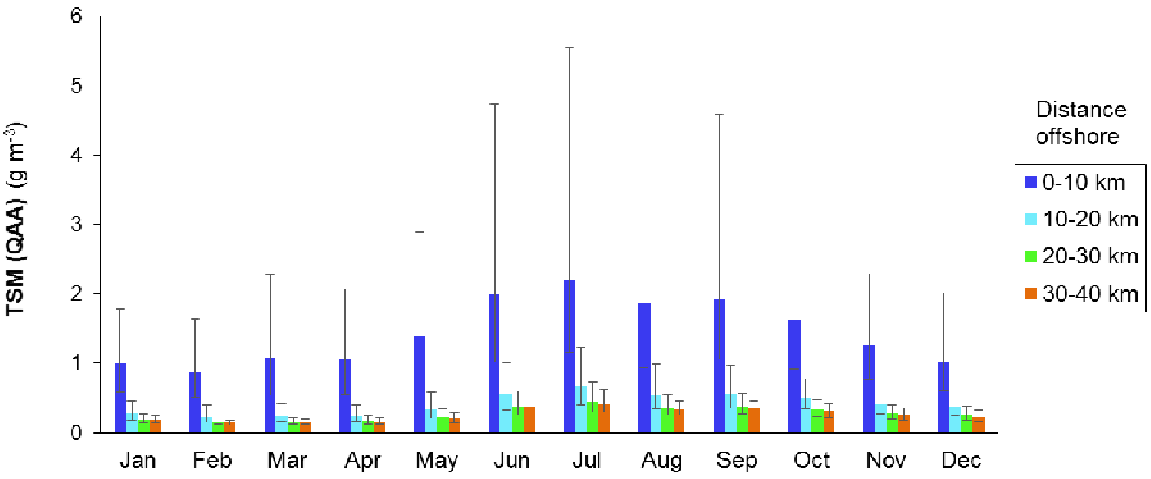

Figure 4-3: Satellite-derived total suspended matter concentration (TSM) in four onshore-offshore bands as shown in Figure 3-6. The coloured bars show median concentrations and the error bars indicate upper and lower quartiles.

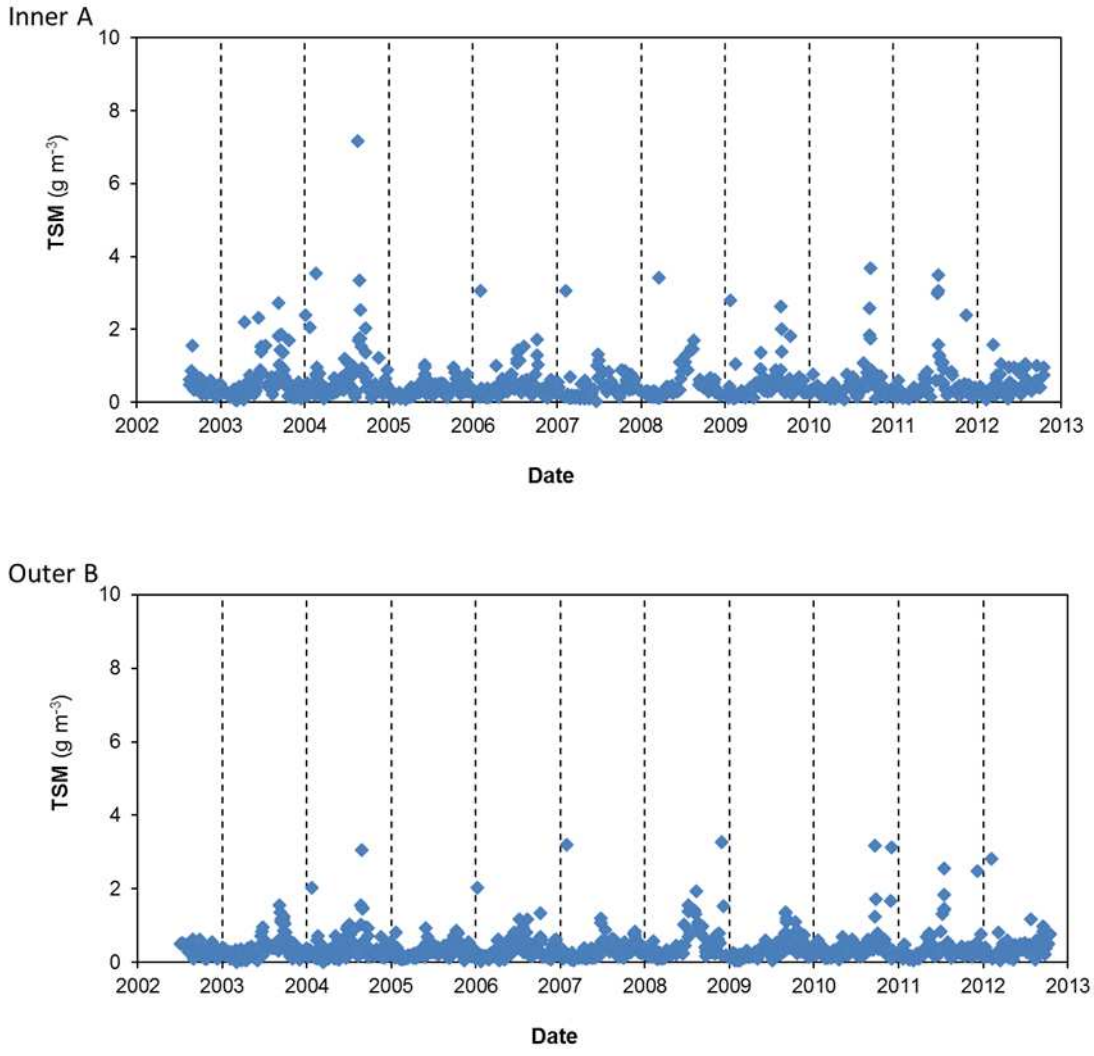

Figure 4-4: Ten-year time-series of satellite-derived total suspended matter (TSM) at inner and outer release sites (labeled A, B in Figure 1-1).

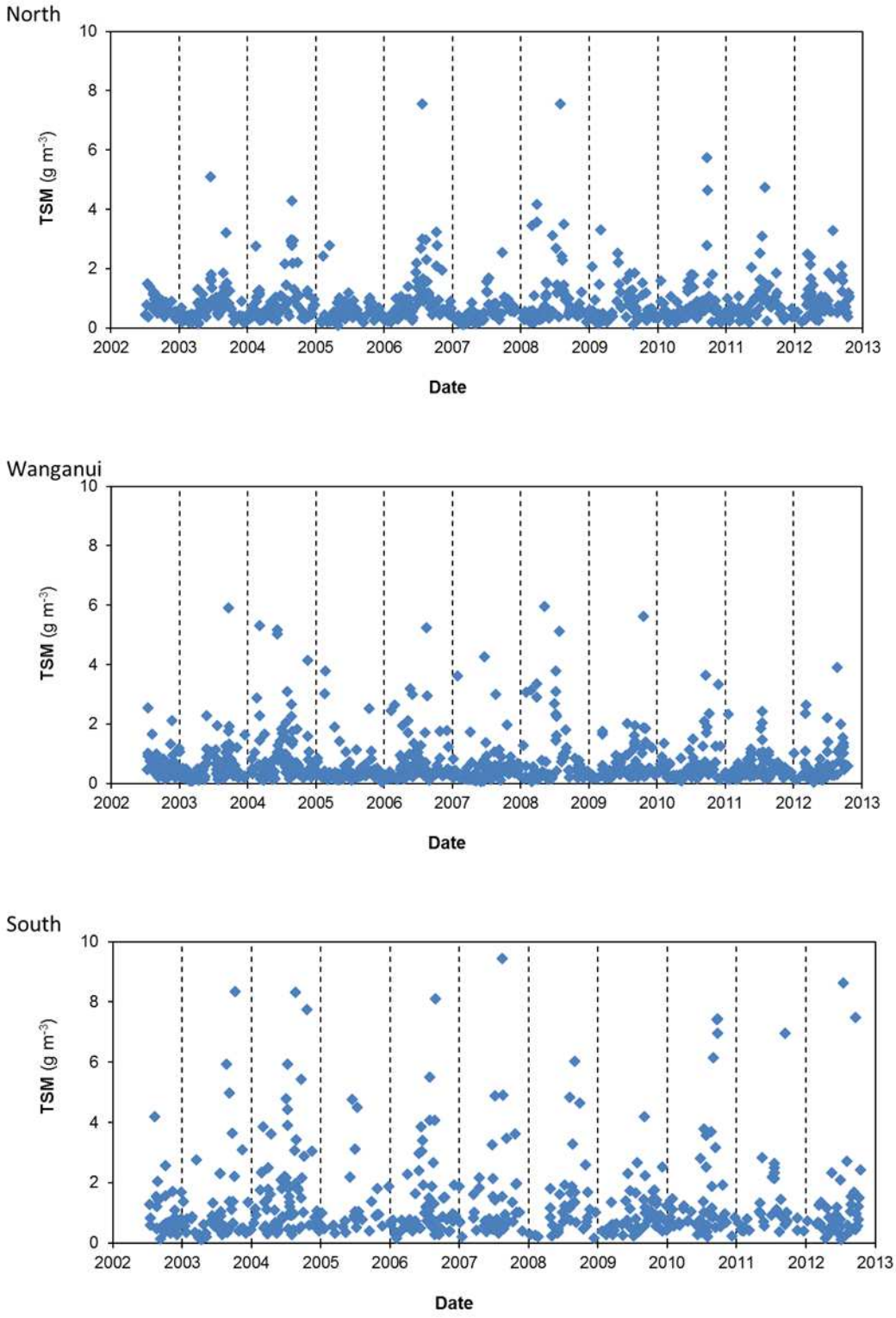

Figure 4-5: Ten-year time-series of satellite-derived total suspended matter (TSM) in the South Taranaki Bight at north, south and Wanganui mouth (sites labelled N, S, W in Figure 1-1).

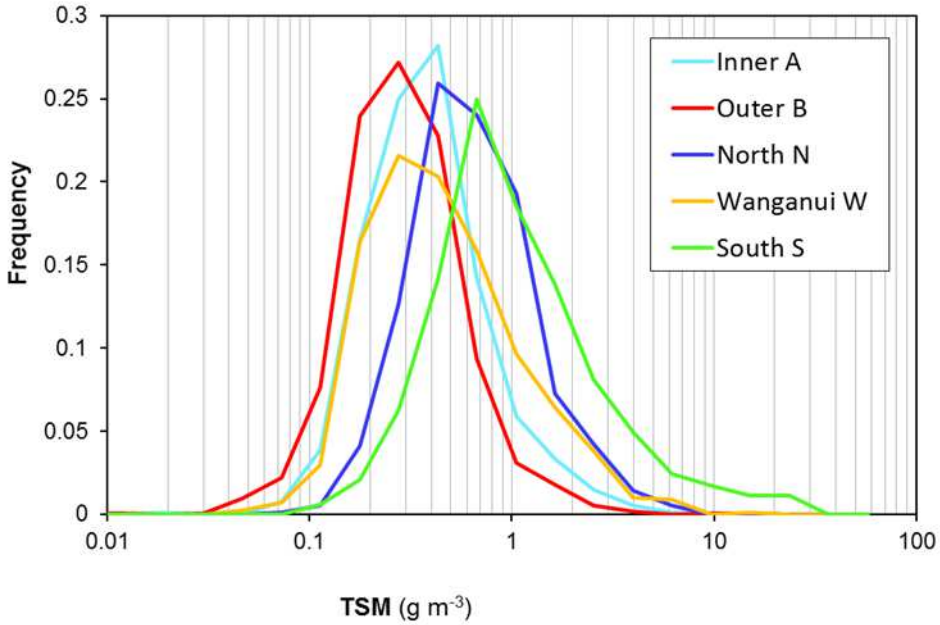

Figure 4-6: Frequency distributions of the ten-years of satellite- derived total suspended matter (TSM) in the South Taranaki Bight at sites labelled A, B, N, W, S in Figure 1-1.

4.2 Proportion of time turbid

The 10-year MODIS dataset of TSM was used to generate spatial and seasonal information on the proportion of the time that waters in the South Taranaki Bight have more than a moderate concentration of suspended sediment (here set to TSM > 3 g m^{-3}). The limit of 3 g m^{-3} is illustrative only, and we do not suggest that this has any particular ecological or optical significance. The long-term average is provided in Figure 4-7. The seasonal and spatial (onshore-offshore) variability in the proportion of the time for which total suspended matter is greater than 3 g m^{-3} in four onshore-offshore bands (Figure 2-2) is shown in Figure 4-8.

Consistent with the maps of TSM concentrations, there is an inshore zone of width about 5 km which has TSM concentration >3 g m^{-3} for more than half of the time, a transition zone to about 10 km offshore which is intermittently turbid (~10-30% of the time), and an offshore zone (more than 10 km offshore) which is rarely turbid (>3 g m^{-3} for only a few days a year).

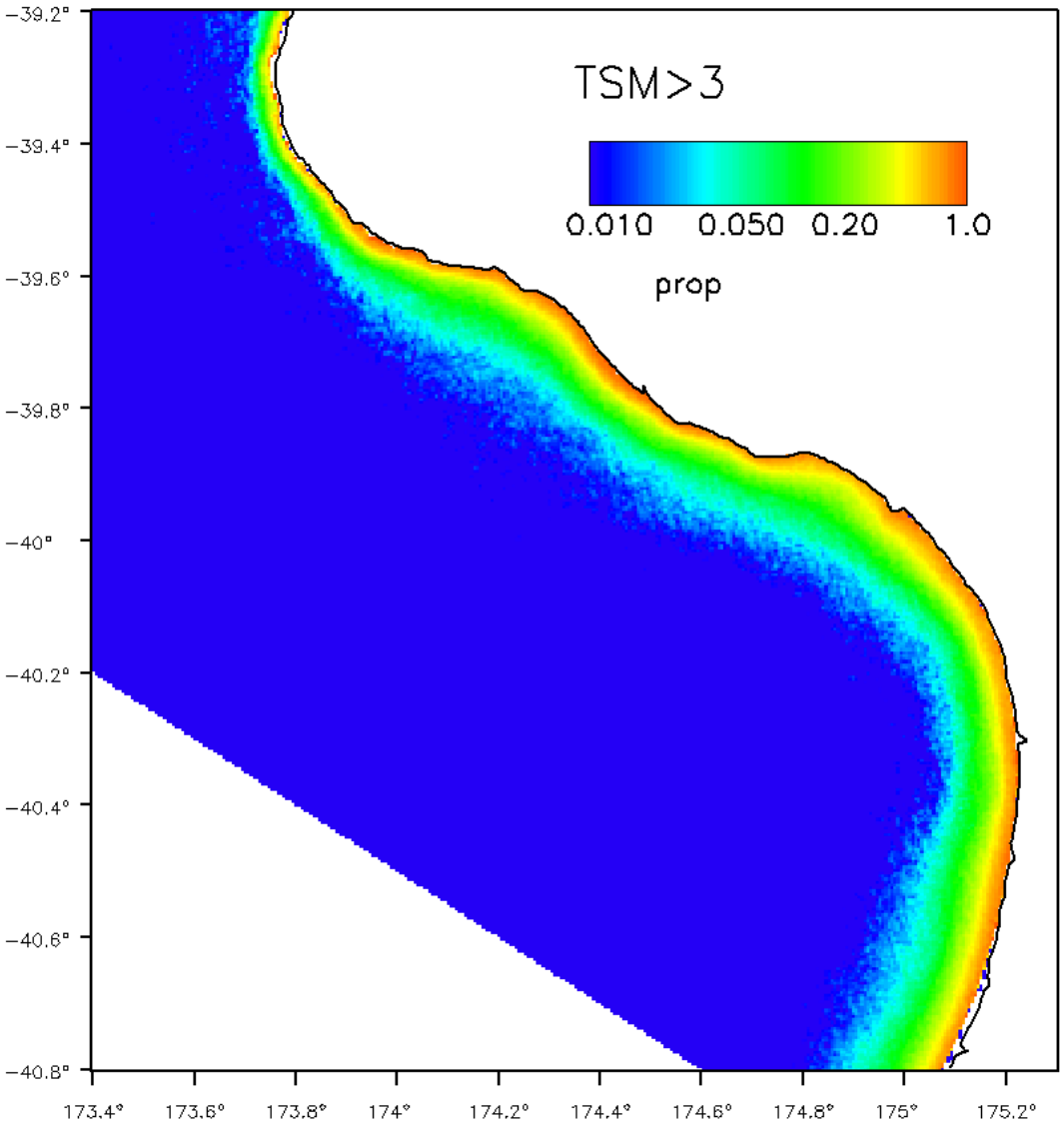

Figure 4-7: Spatial distribution of the proportion of the time for which total suspended matter (TSM) is greater than 3 g m^{-3}. Long term averages are calculated as the mean value over ten years of MODIS-Aqua data. Note that the colour scale is logarithmic.

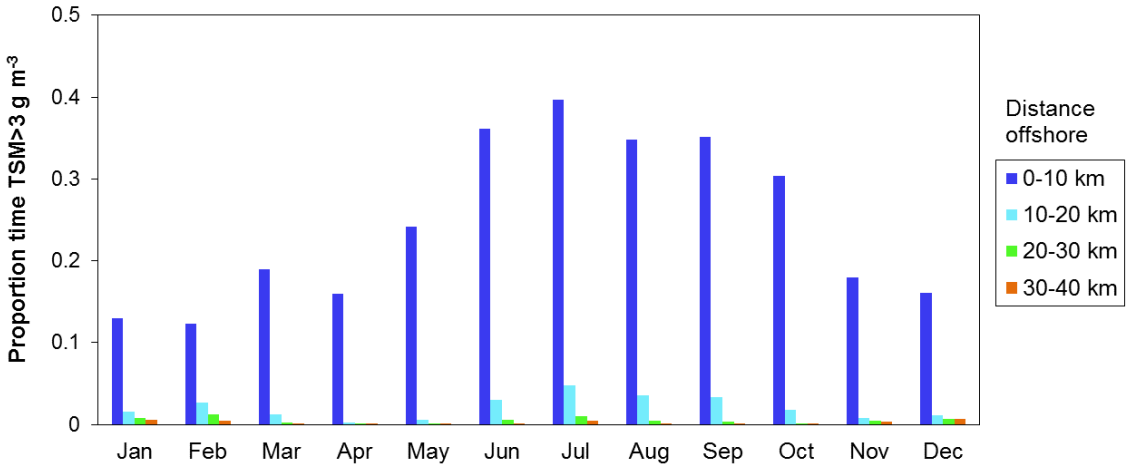

Figure 4-8: Mean proportion of the time for which total suspended matter is greater than 3 g m^{-3}, in four onshore-offshore bands as shown in Figure 3-6.

5 Objective 4: Satellite chlorophyll-a

The decadal mean distribution map for near-surface chlorophyll-a concentration (chl-a) as a proxy for phytoplankton abundance is shown in Figure 5-1. These were generated by applying a local scaling to absorption by phytoplankton at 488 nm produced by the QAA algorithm applied to 10 years of MODIS-Aqua data. The monthly climatologies of chl-a are shown in Figure 5-2 and the means by distance offshore are shown in Figure 5-3. Data from the 10 year MODIS records were extracted at the inner (A) and outer (B) mining sites (Figure 1-1) - Figure 5-4. Similarly, Figure 5-5 shows the 10-year time-series of satellite-derived chl-a at the three coastal sites located to the north, south and centrally at the Wanganui River mouth (labeled N, W, S in Figure 1-1).

The long-term average near surface chl-a concentration was highest (long-term medians up to 5 mg m^{-3}) less than 5 km of the coast. Median chl-a concentrations rapidly decreased with distance offshore to an open-water annual median of ~0.3 mg m^{-3} (annual interquartile range 0.09-0.5 mg m^{-3}) more than 10 km from the coast. There was a seasonal cycle in monthly median chl-a, with higher concentrations in winter (median 0.35 mg m^{-3} in May for 0–40 km offshore) and lower values in summer (minimum mean of 0.15 mg m^{-3} in February for 0–40 km offshore). More than 10 km from the coast, the STB was characterized by phytoplankton blooms and these offshore blooms were often large and intense (see examples in Appendix B: Figure 11-1, Figure 11-2, Figure 11-3). Phytoplankton blooms closer to the coast were also observed occasionally (Appendix B: Figure 11-4). Peak chl-a concentrations within these blooms often exceeded 4 mg m^{-3}. Over the past ten years at the 6 selected sites, there has been no temporal trend in chl-a concentration ($p > 0.01$).

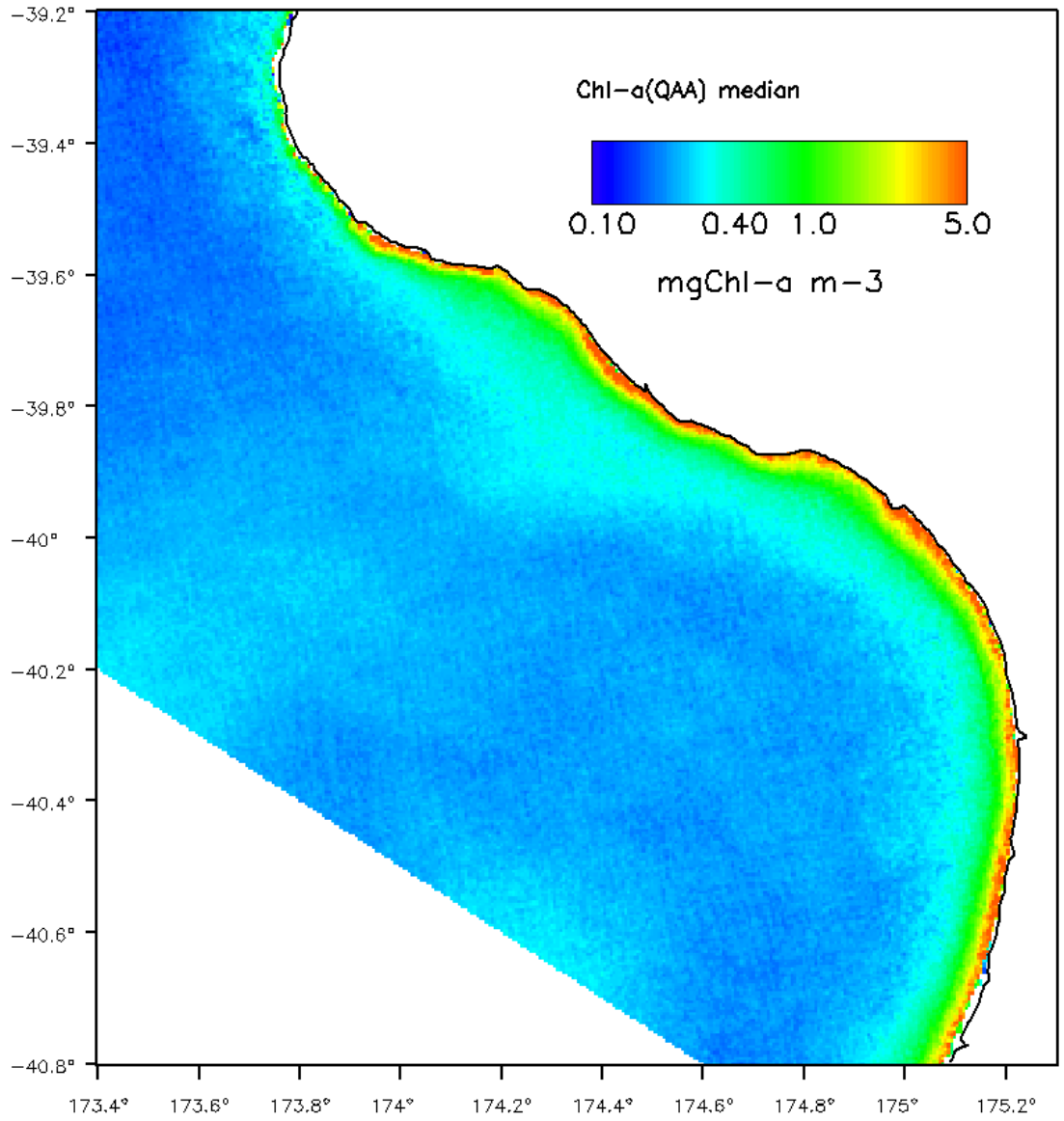

Figure 5-1: Spatial distribution of median near-surface chlorophyll-a concentration (chl-a, mg m^{-3}) based on algal absorption at 488 nm from the QAA algorithm. Medians were calculated from all MODIS-Aqua data between 2002 and 2012.

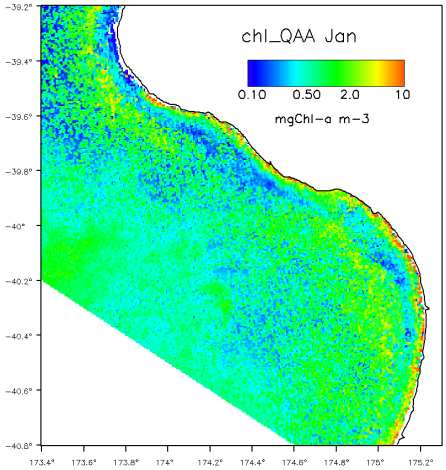
chl_QAA Jan
0.10 0.50 2.0 10
mgChl-a m-3

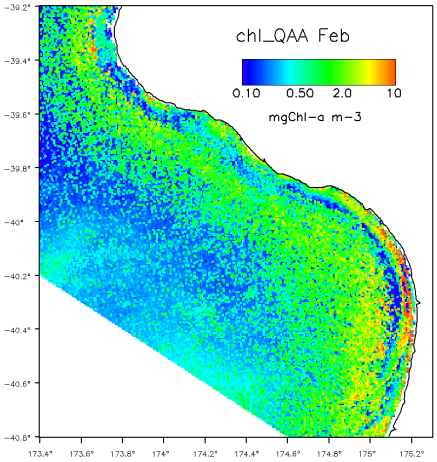
chl_QAA Feb
0.10 0.50 2.0 10
mgChl-a m-3

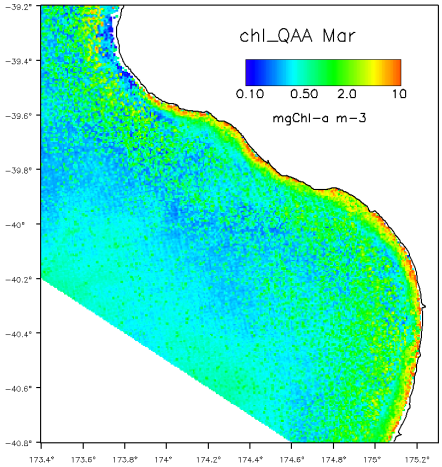
chl_QAA Mar
0.10 0.50 2.0 10
mgChl-a m-3

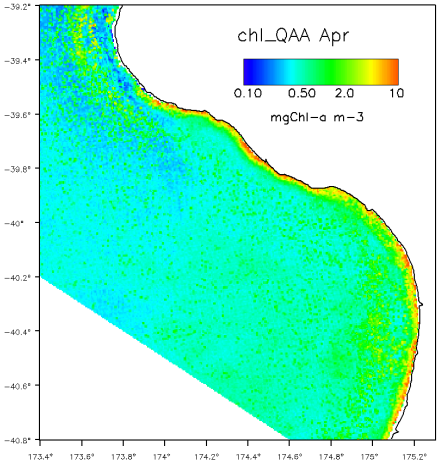
chl_QAA Apr
0.10 0.50 2.0 10
mgChl-a m-3

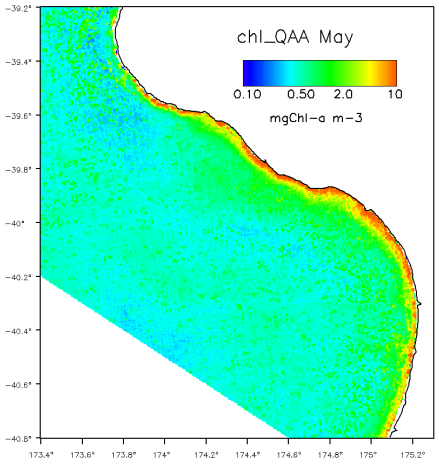
chl_QAA May
0.10 0.50 2.0 10
mgChl-a m-3

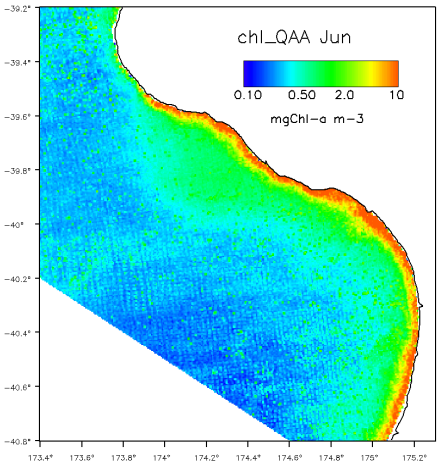
chl_QAA Jun
0.10 0.50 2.0 10
mgChl-a m-3

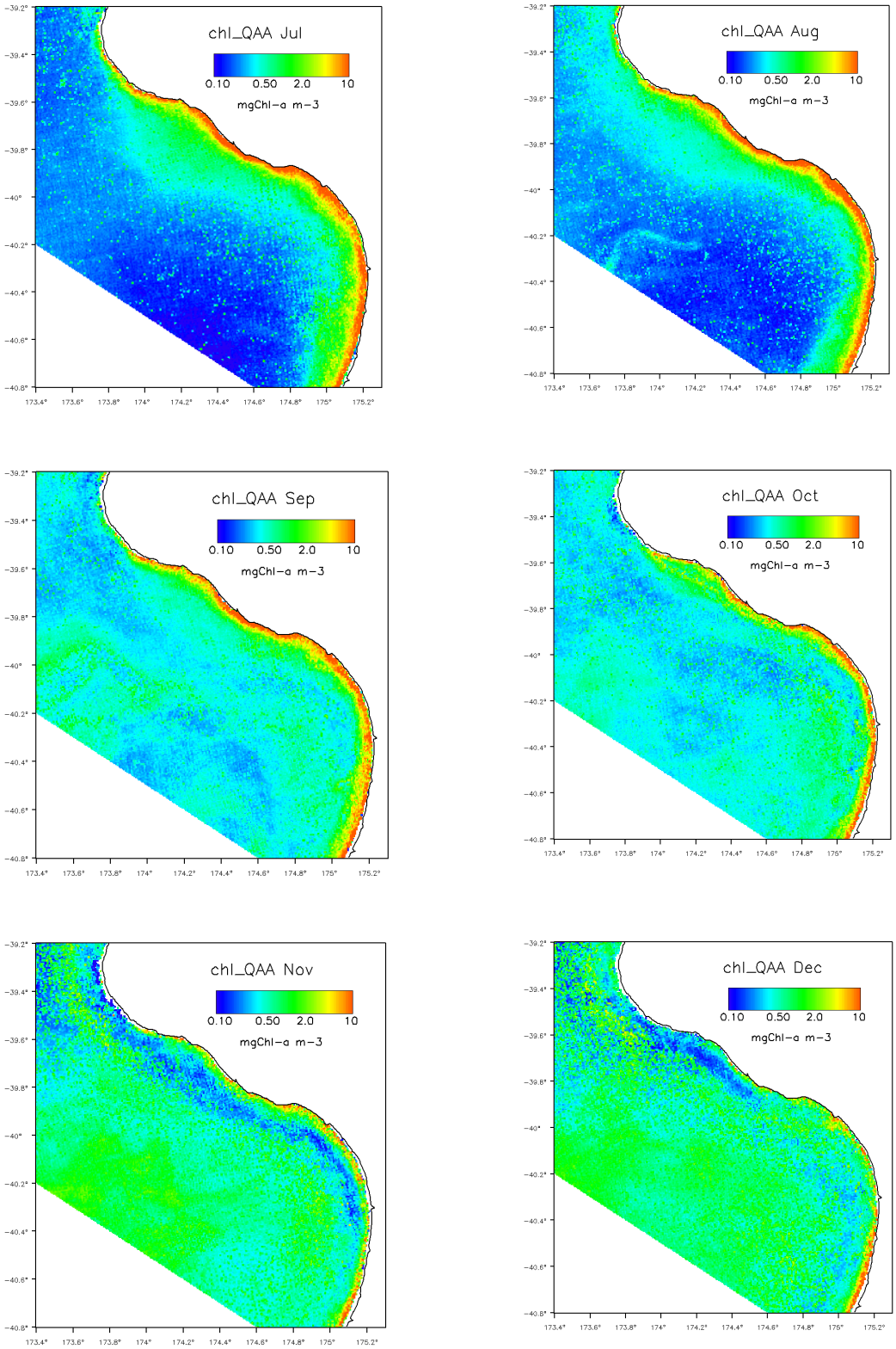

Figure 5-2: Monthly mean climatology of near surface chlorophyll-a concentration (chl-a, mg m^{-3}) based on algal absorption at 488 nm from the QAA algorithm applied to MODIS-Aqua data over the period 2002 to 2012.

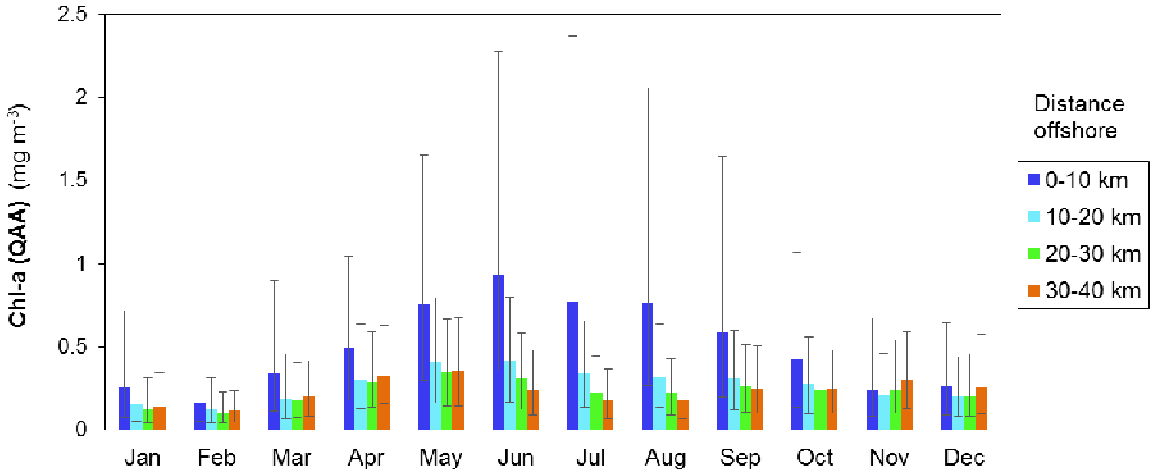

Figure 5-3: Chlorophyll-a concentration (chl-a, mg m^{-3}) observed by MODIS-Aqua in 4 onshore-offshore bands as shown in Figure 3-6. The coloured bars show median concentrations and the error bars indicate upper and lower quartiles.

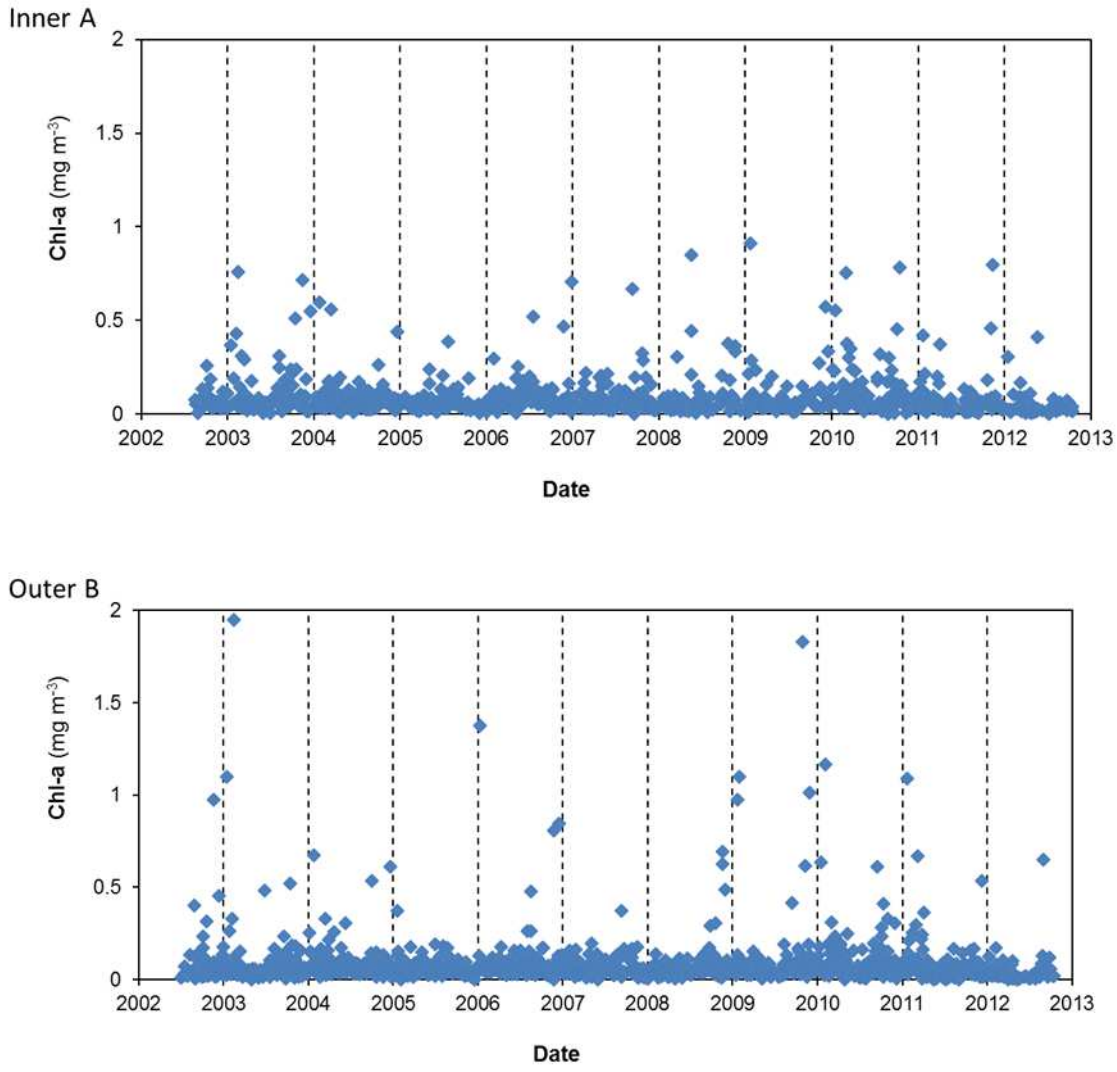

Figure 5-4: Satellite-derived chl-a concentration values for the inner and outer mining sites for the period 2002 to 2012 (sites are labelled A and B in Figure 1-1).

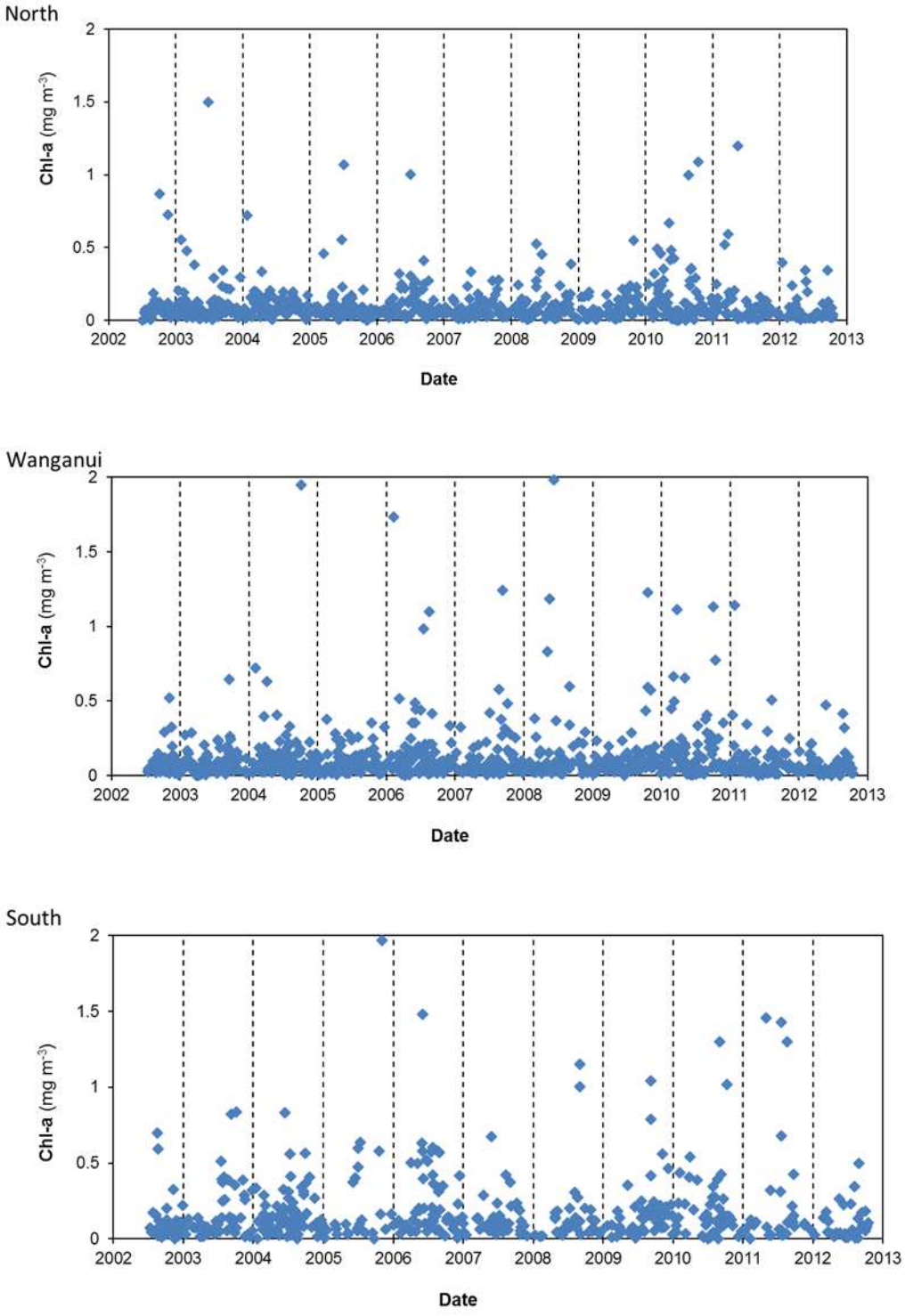

Figure 5-5: Satellite-derived chl-a concentration values for the northern, southern and Wanganui River mouth sites, for the period 2002 to 2012. Sites are labelled N, S, W in Figure 1-1.

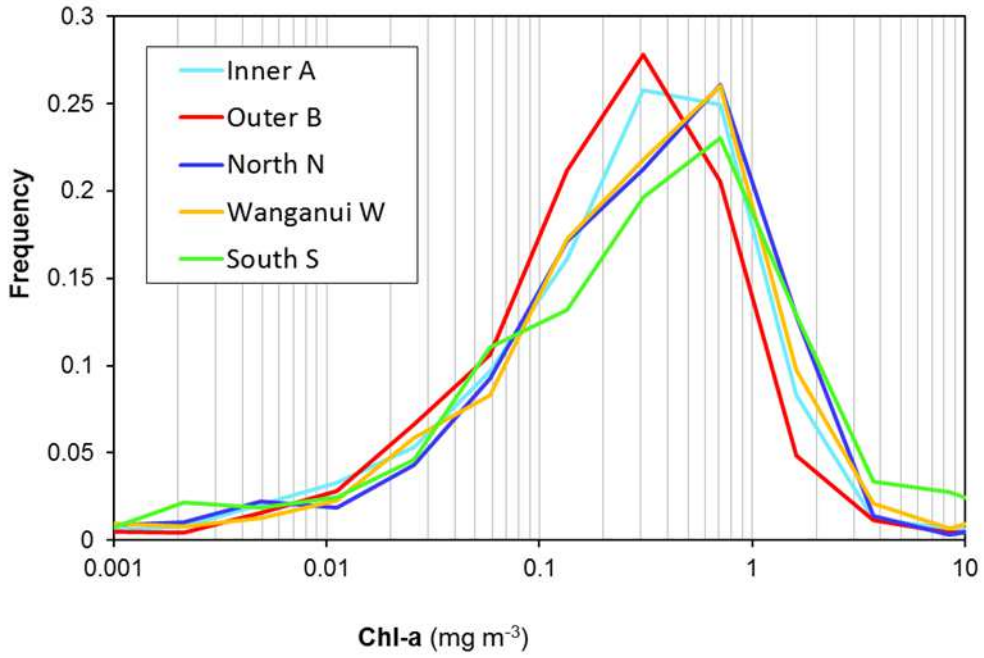

Figure 5-6: Frequency distributions of the ten-years of satellite-derived chl-a (mg m^{-3}) in the South Taranaki Bight at sites labelled A, B, N, W, S in Figure 1-1.

6 Objective 5: Satellite CDOM absorption

Based on MODIS-Aqua observations from 2002-2012, CDOM absorption is distributed through the STB as shown in Figure 6-1. The monthly CDOM absorption climatology is shown in Figure 6-2 and summarised in Figure 6-3. There is a narrow band (<5 km wide) of persistently high CDOM absorption (>0.5 m^{-1} at 412 nm) along the STB coast. Beyond this, the CDOM absorption at 412 nm is relatively homogenous spatially, with a background level of about 0.05 m^{-1}. There is no clear annual cycle of CDOM absorption in the four offshore bands, though median values were highest in October. Higher values of CDOM absorption in the near-coast zone are likely to be due principally to CDOM outflow from rivers. The contribution from breakdown of autochthonous phytoplankton productivity is likely to be relatively low in the STB. More than 10 km offshore, CDOM absorption is likely to be driven mainly by seasonal variations in phytoplankton production and breakdown. Figure 6-4 shows the ten-year time-series of satellite-derived CDOM absorption at two mining sites labeled A and B in Figure 1-1). Figure 6-5 shows the ten-year time-series of satellite-derived CDOM absorption at the three coastal sites located to the north, south and centrally at the Wanganui River mouth (labeled N, W, S in Figure 1-1). The statistical distribution of CDOM absorption at each of these 6 sites is summarized in Figure 6-6. Median values are around 0.1 m^{-1} at all sites, with very few measurements >1 m^{-1} or <0.01 m^{-1}.

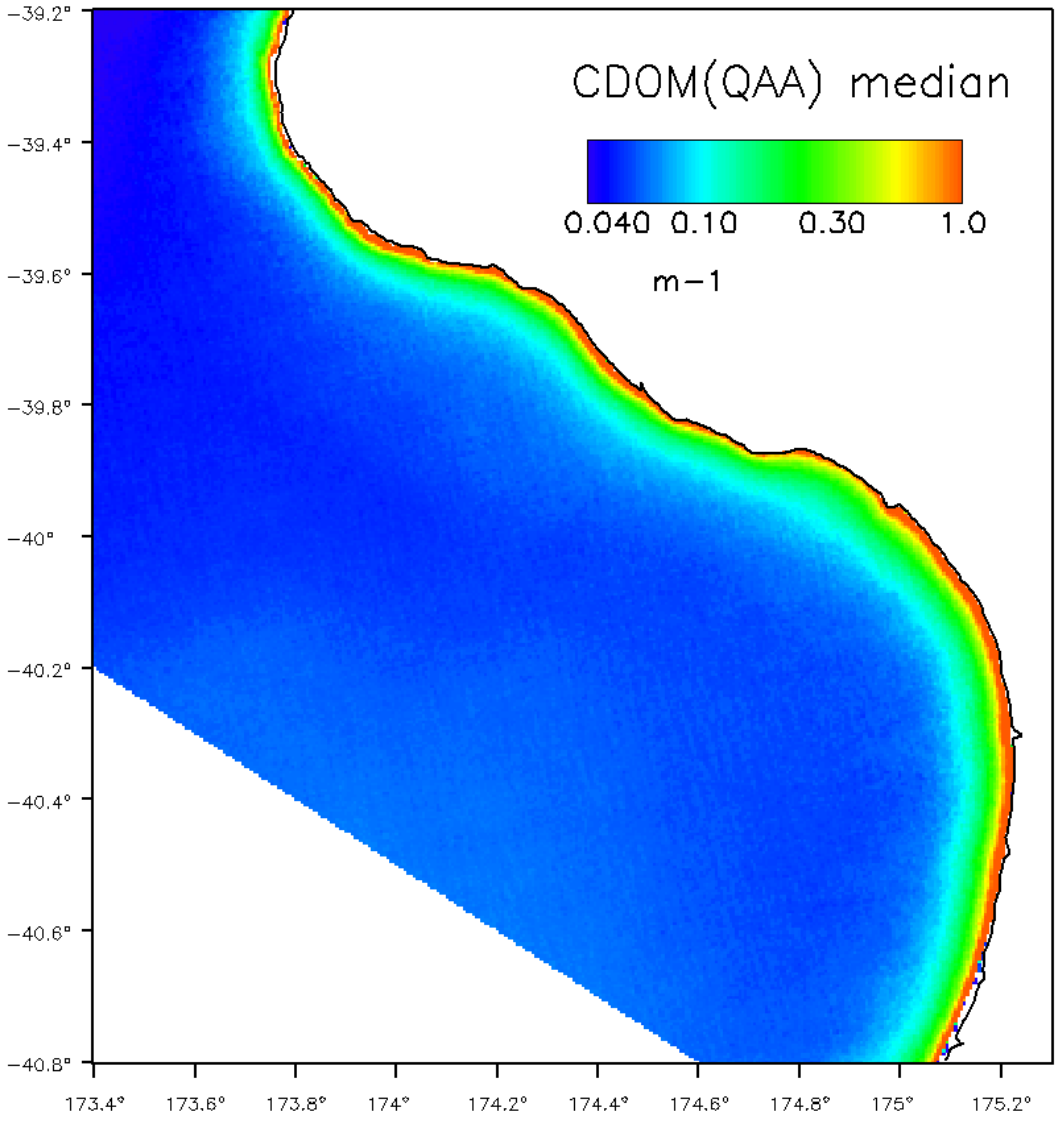

Figure 6-1: Spatial distribution of long-term median CDOM absorption at 412 nm based on the ADET412 product from the QAA algorithm corrected for absorption by non-algal particles. The median value was based on ten years of MODIS-Aqua data, 2002-2012.

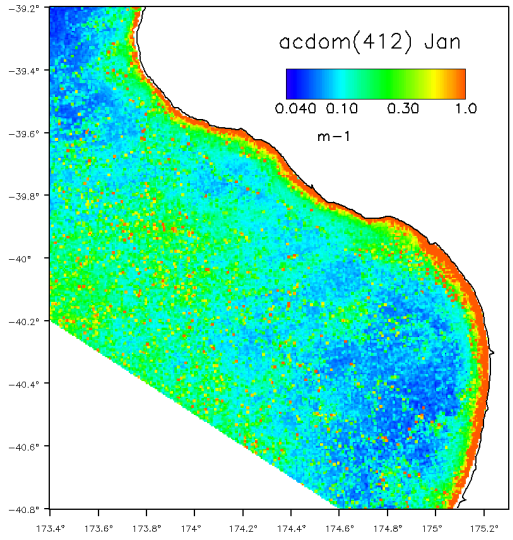
acdom(412) Jan
0.040 0.10 0.30 1.0
m−1

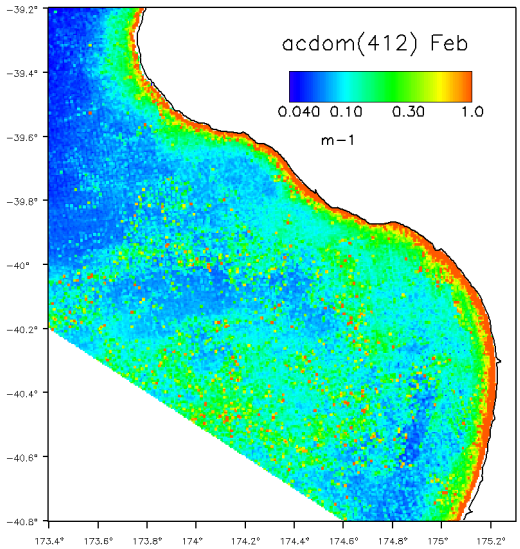
acdom(412) Feb
0.040 0.10 0.30 1.0
m−1

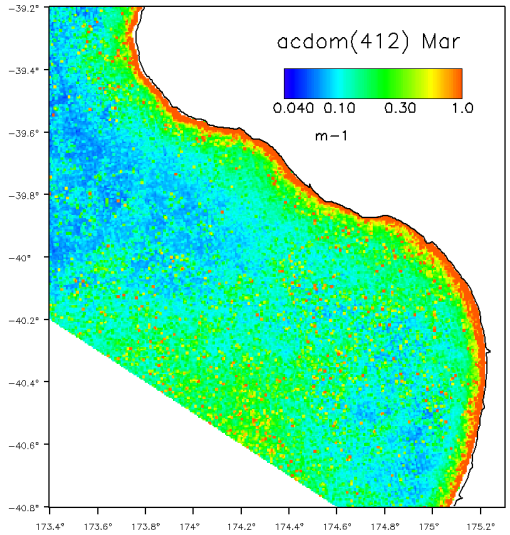
acdom(412) Mar
0.040 0.10 0.30 1.0
m−1

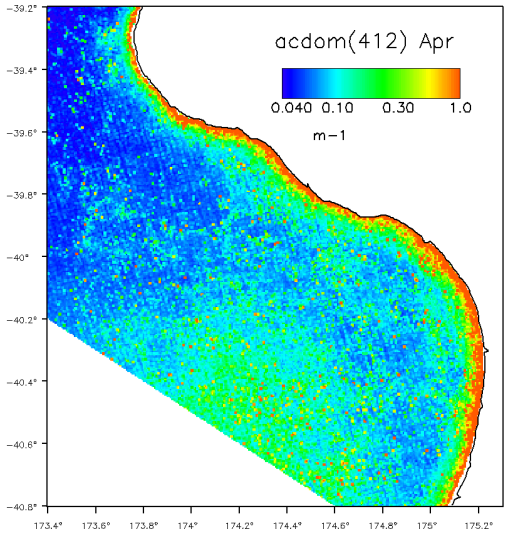
acdom(412) Apr
0.040 0.10 0.30 1.0
m−1

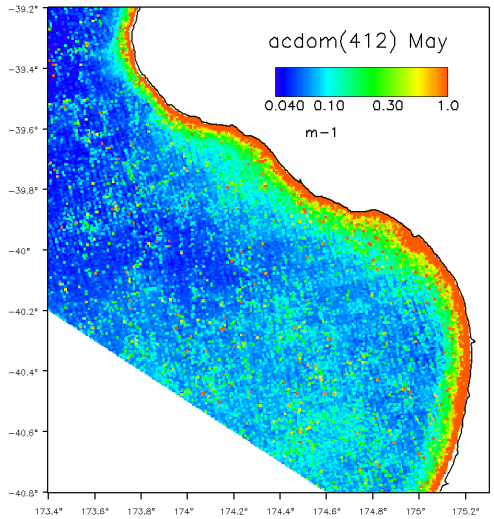
acdom(412) May
0.040 0.10 0.30 1.0
m−1

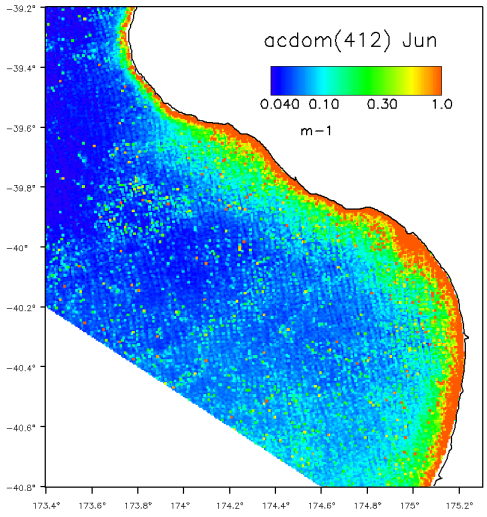
acdom(412) Jun
0.040 0.10 0.30 1.0
m−1

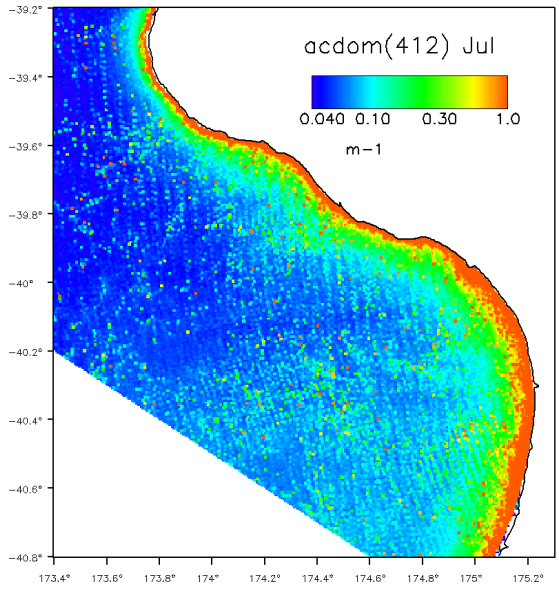
acdom(412) Jul
0.040 0.10 0.30 1.0
m−1
−39.2°
−39.4°
−39.6°
−39.8°
−40°
−40.2°
−40.4°
−40.6°
−40.8°
173.4° 173.6° 173.8° 174° 174.2° 174.4° 174.6° 174.8° 175° 175.2°

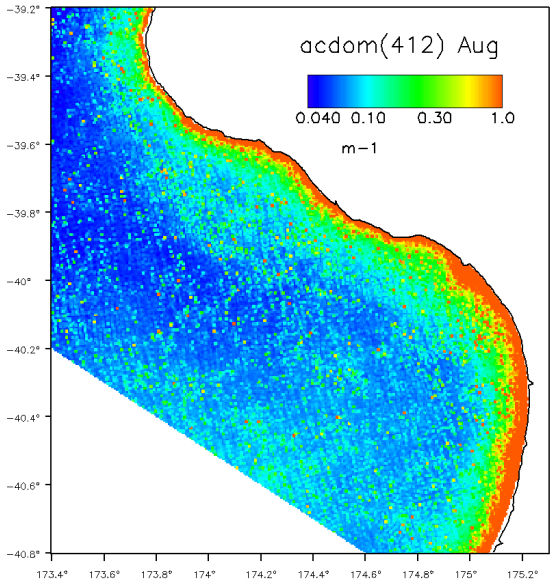
acdom(412) Aug
0.040 0.10 0.30 1.0
m−1
−39.2°
−39.4°
−39.6°
−39.8°
−40°
−40.2°
−40.4°
−40.6°
−40.8°
173.4° 173.6° 173.8° 174° 174.2° 174.4° 174.6° 174.8° 175° 175.2°

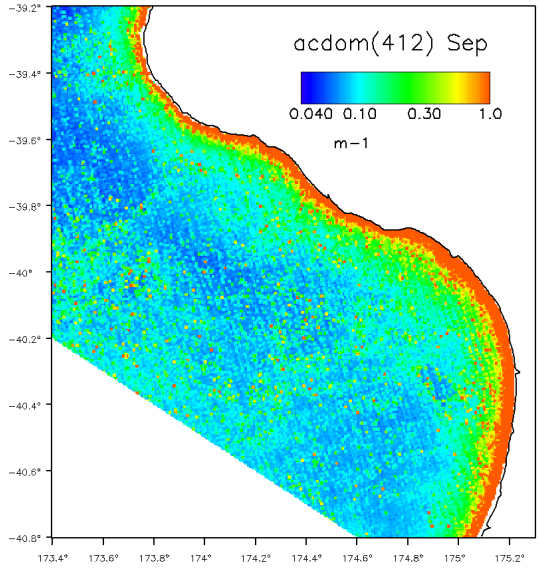
acdom(412) Sep
0.040 0.10 0.30 1.0
m−1
−39.2°
−39.4°
−39.6°
−39.8°
−40°
−40.2°
−40.4°
−40.6°
−40.8°
173.4° 173.6° 173.8° 174° 174.2° 174.4° 174.6° 174.8° 175° 175.2°

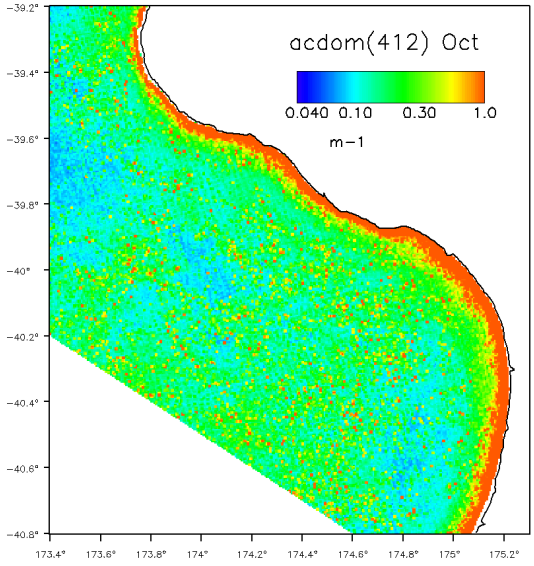
acdom(412) Oct
0.040 0.10 0.30 1.0
m−1
−39.2°
−39.4°
−39.6°
−39.8°
−40°
−40.2°
−40.4°
−40.6°
−40.8°
173.4° 173.6° 173.8° 174° 174.2° 174.4° 174.6° 174.8° 175° 175.2°

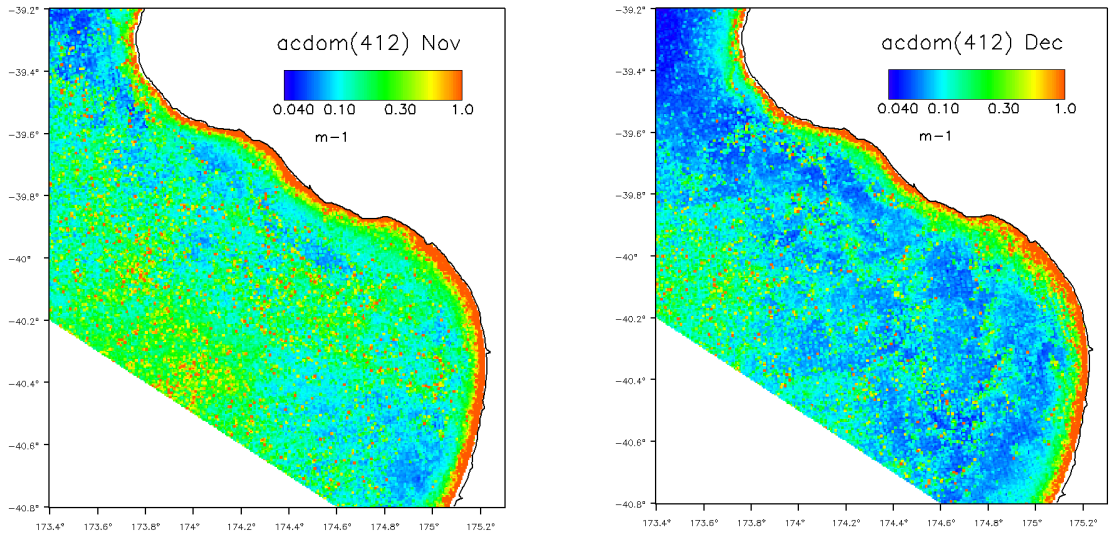

Figure 6-2: Monthly climatology of CDOM absorption at 412 nm based on the ADET412 product from the QAA algorithm corrected for absorption by non-algal particles. Monthly averages are calculated as the mean value in each month over ten years of MODIS-Aqua data, 2002-2012.

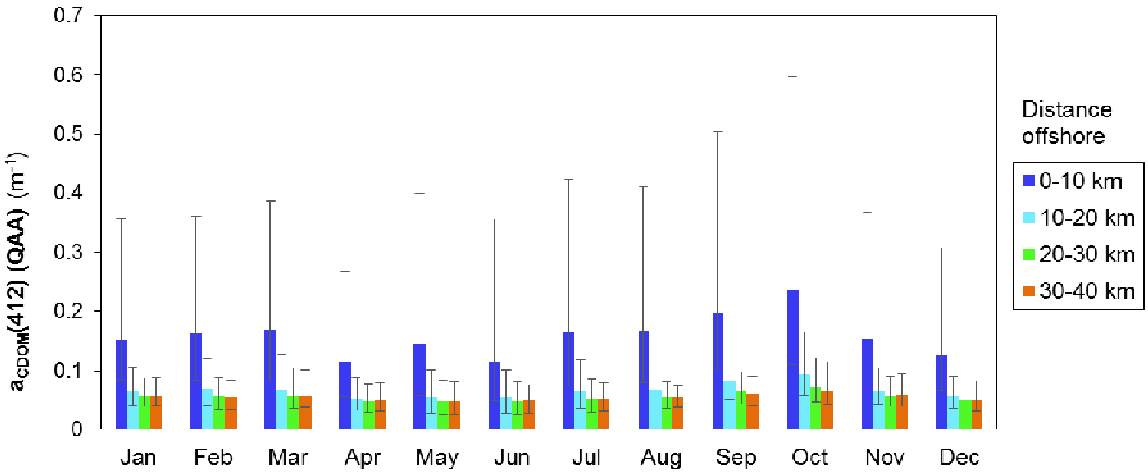

Figure 6-3: Satellite-derived absorption by coloured dissolved organic matter (CDOM) at 412 nm in 4 onshore-offshore bands as shown in Figure 3-6. The main coloured bars show median values and the error bars indicate upper and lower quartiles.

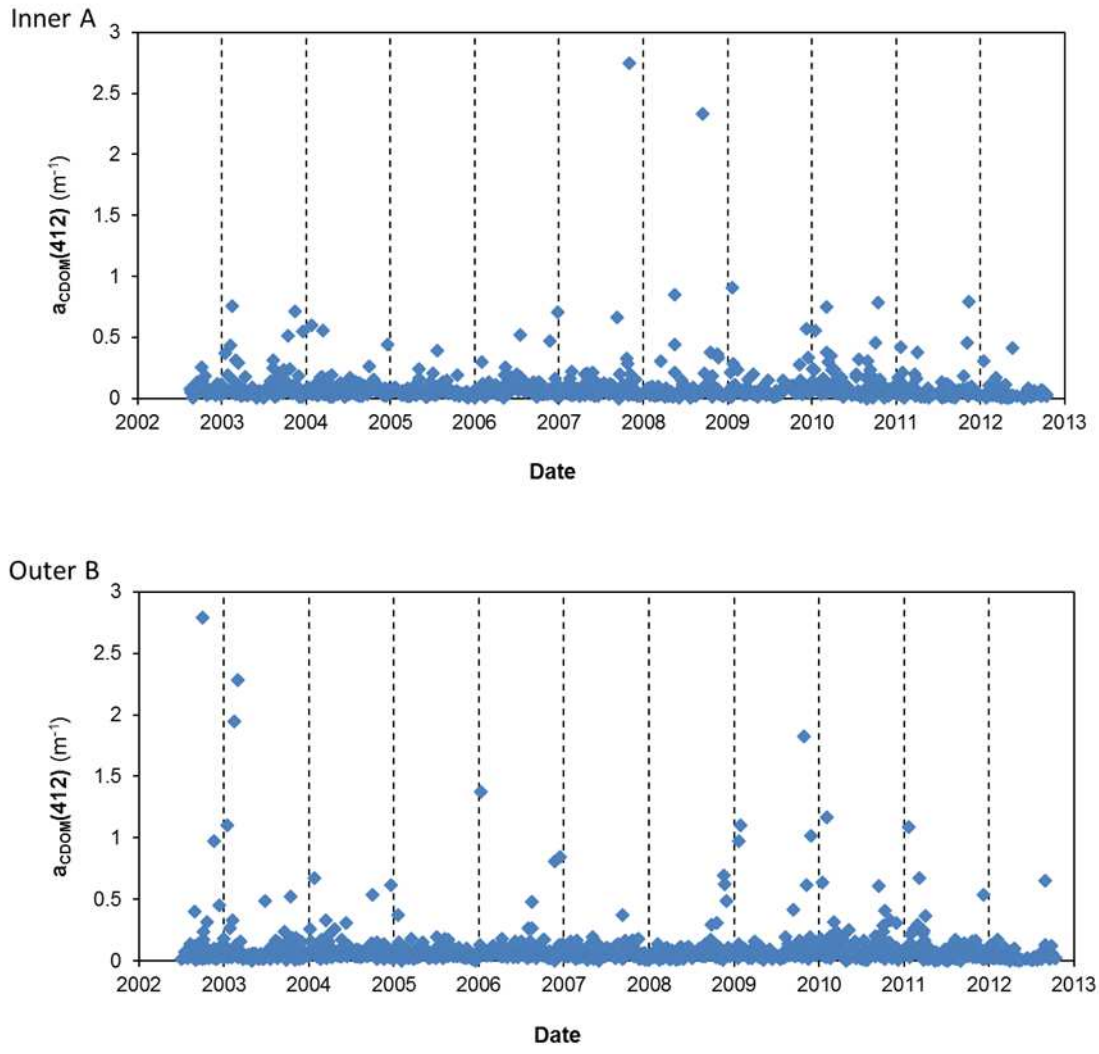

Figure 6-4: Ten-year time-series of satellite-derived CDOM absorption at 412 nm at inner and outer mining sites (labeled A and B in Figure 1-1) based on ten years of MODIS-Aqua data, 2002-2012.

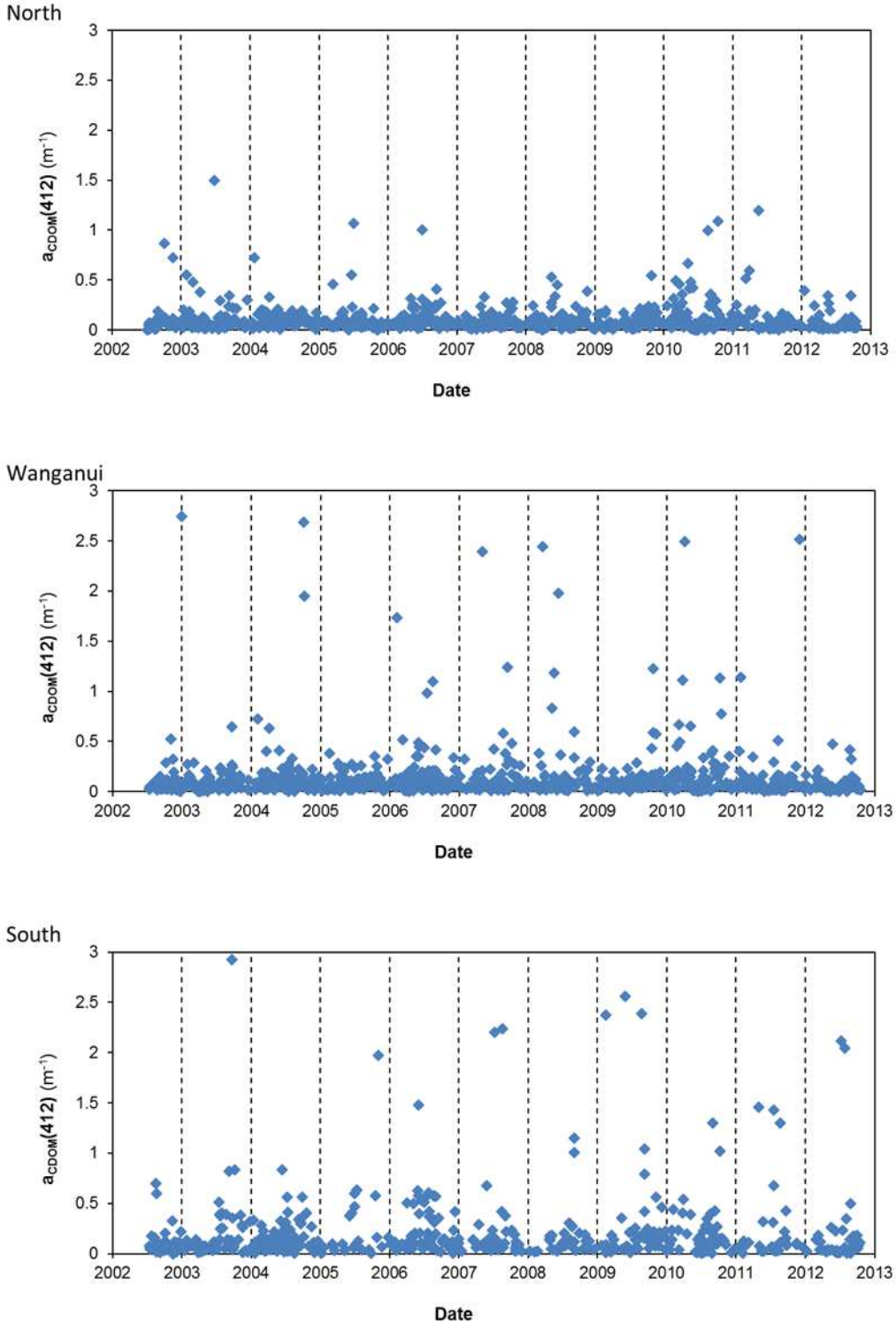

Figure 6-5: Ten-year time-series of satellite-derived CDOM absorption at 412 nm at 3 sites: north, south and Wanganui river mouth sites (labelled N, W, S in Figure 1-1) based on ten years of MODIS-Aqua data, 2002-2012.

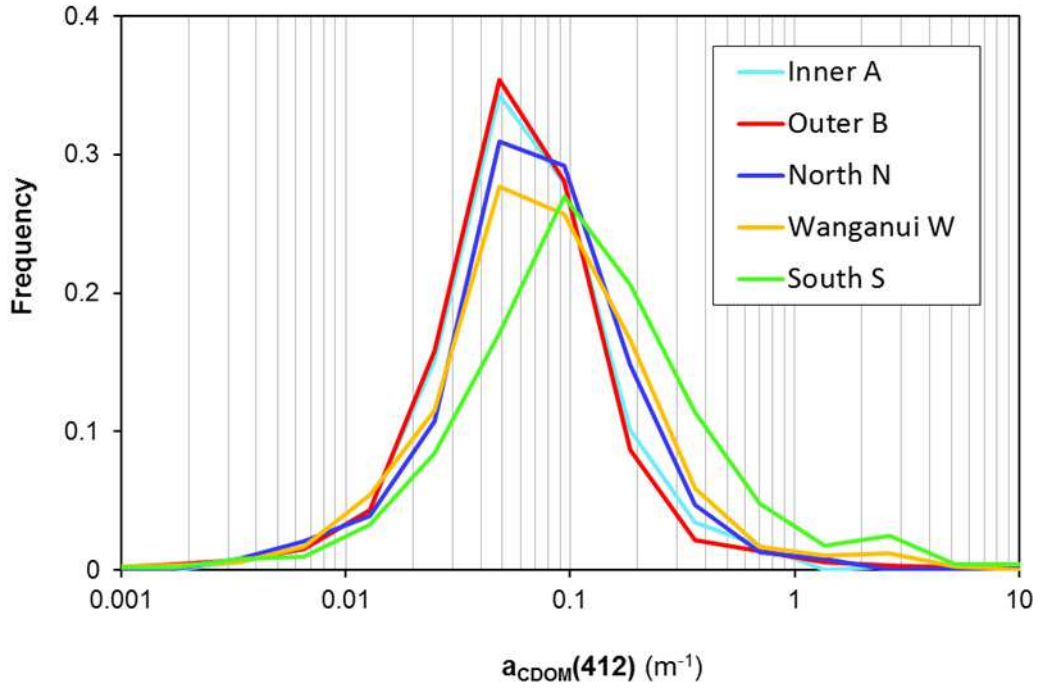

Figure 6-6: Frequency distributions of satellite-derived CDOM absorption at 412 nm in the South Taranaki Bight (sites labelled A, B, N, W, S in Figure 1-1) based on ten years of MODIS-Aqua data, 2002-2012.

7 Discussion and conclusions

Some important limitations of the satellite-based approach should be noted:

- Ocean colour sensors only see material in the upper water column, typically from a few cm to a few metres of depth, depending on the turbidity of the water. In highly turbid waters, the satellite may only see material in upper few centimetres, whereas in waters with lower turbidity, the satellite may see material in the upper tens of metres. Deeper suspended sediment and that near the sea-bed will usually not be seen in satellite data.
- Satellite in-water algorithms assume optically-deep water i.e. that reflection of light from the sea bed is small compared to reflection by water constituents. This is likely to be true over the study area.
- Satellite observations of TSM, chl-a and absorption by non-algal particles and CDOM are inherently less accurate than *in situ* measurements. In particular, estimates of chl-a in the presence of moderate concentrations of sediment are

uncertain because the subtle effect of chl-a on ocean colour is masked by the stronger effect of sediment.

- Ocean colour satellite data are not obtained for areas obscured by clouds, and some clouds are present most of the time in the STB. In our data analysis, about 13% of the satellite observations were completely cloud free. As concentrations of optically active material in the water column are related to the probability of cloud present/absence, there is a bias in climatologies based on satellite data. For example, concentrations of suspended sediment in the coastal zone are likely to be highest just after high rainfall events (elevated land-run off) and/or when high winds/high waves are present (higher coastal erosion and sediment resuspension). These situations are likely to occur when clouds prevent ocean colour satellites seeing the water surface. Hence, climatologies of TSM based on satellite data are likely to underestimate the actual long-term mean concentrations.

Notwithstanding these caveats, satellite observation of ocean colour is an effective tool at providing large-area (100s of km), long-term (years to decades) observations of coloured material in coastal zones. Water sampling from vessels or moorings, though providing more accurate data, has limited ability to assess or monitor these large-scale patterns over long periods.

The main findings of this study are given below in numbered form for clarity.

1. The specific inherent optical properties (sIOPs) were found to be indistinguishable among surface water samples collected along the southern ("Mana") to northern STB. Phytoplankton communities were found to vary along the STB coast but the effect of this on chl-a algorithm performance is expected to be low. Hence, *in situ* data in the Mana region can be used to validate and tune satellite algorithms applicable to the STB.

2. Atmospheric correction of satellite data was carried out using the NIR/SWIR switching algorithm (Wang & Shi, 2007), which performs pixel-by-pixel correction and is valid in turbid waters. Satellite observations of water reflectance spectra were converted to three key IOPs using the Quasi-Analytical Algorithm (QAA update v5: Lee et al., 2002; Lee et al., 2009). These IOPs were converted to geophysical parameters using locally-tuned and/or validated relationships: (a) chl-a concentration (proxy for phytoplankton biomass) was obtained from a scaling of the absorption of phytoplankton at 488 nm (QAA product APH488). Conversion factors from Bricaud et al. (1995) were used and these were successfully validated against local measurements in the STB; (b) TSM was obtained from a scaling of particulate backscattering at 488 nm (QAA product BBP488). The conversion factor used was derived from local measurements of backscattering by non-algal particles in the STB region. Spatial variation in the particle size spectrum of naturally-occurring material means that TSM is likely to be underestimated close to the shore (by ~40%) and overestimated offshore (by ~60%). This uncertainty is small compared to the variation in TSM concentrations across the domain (>2 orders of magnitude); (c) absorption by CDOM at 412 nm was estimated by correcting the total (i.e. particulate and dissolved) detrital absorption at 412 nm (QAA product ADET412) for absorption due to NAP alone. The correction factor was derived from measurements of NAP absorption in the STB region.

3. End-to-end comparisons between *in situ* and satellite observations of chl-a concentration, TSM concentration and absorption by CDOM in the STB give good confidence that the satellite data presented in this study are fit for purpose.

4. Values of TSM concentration, chl-a concentration and CDOM absorption are highest within a few km of the coast and rapidly decrease with increasing distance offshore to about 10 km. Beyond this distance offshore, the spatial structure in the long-term mean (climatological) variation in TSM concentration, chl-a concentration and CDOM absorption is relatively weak. However, individual satellite images (Appendix B) show that there is substantial short-term, small-scale variation in these properties in the STB, associated with a combination of local production processes ("phytoplankton blooms"), river discharge, resuspension of sediment from the sea-bed and/or coastal erosion and transport. The dataset of satellite observations built up in the project is available for interrogation regarding these processes as required.

5. According to the satellite data, the median concentration of TSM in the 0–10 km offshore band was 1.4 g m^{-3} over an annual cycle, with a maximum monthly median of 1.9 g m^{-3} in September and minimum of 0.9 g m^{-3} in February. In the region of the STB between 10 and 40 km offshore, monthly median TSM concentrations were 0.15–0.67 g m^{-3}. In the 0-10 km offshore band, TSM was greater than 3 g m^{-3} about 27% of the time over a year (between 12% and 40% by month). Further offshore, TSM was greater than 3 g m^{-3} rarely (less than 5% of the time). There was substantial short-term and small-area variability in TSM observed in the satellite data; annual interquartile range of TSM between 0 and 10 km offshore was 0.8 – 3.2 g m^{-3}. At the three selected inshore sites, peak sediment concentrations in the 10-year record were 8 g m^{-3} (north south station N), 13 g m^{-3} (Wanganui station, W) and 46 g m^{-3} (south station, S). It is not possible to say if these estimates are quantitatively reliable.

6. Elevated chl-a concentrations in the STB seem to be associated with two processes. First, elevated chl-a co-occurs with higher TSM close to the coast. Positive correlation between chl-a and TSM was also seen in the *in situ* data. Long-term median chl-a concentrations were highest (~5 mg m^{-3}) within a few km of the coast, but rapidly decreased with distance offshore to an annual median of 0.22 mg m^{-3}. There was a seasonal cycle in monthly median chl-a concentration, with higher concentrations in May and November (maximum 0.35 mg m^{-3} for 0–40 km offshore) and lower values in summer (minimum mean of 0.15 mg m^{-3} in February for 0–40 km offshore). This is likely to occur because riverine run-off brings sediment and nutrients into the STB, and the nutrients stimulate phytoplankton production. Second, offshore, the STB was characterized by intermittent phytoplankton blooms. These offshore blooms varied in size, but were often spatially large and covered much of the offshore STB. Some blooms may be associated with upstream Farewell Spit dynamics (e.g. Figure 11-1, Figure 11-2, Figure 11-3) and, more rarely, some may be affected by Cook Strait dynamics (Figure 11-4). Both nearshore and offshore blooms could be intense, with chl-a concentrations exceeding 4 mg m^{-3}.

7. Median absorption due to CDOM at wavelength of 412 nm (blue) was highest within a few km of the shore (>0.5 m^{-1}), decreasing to a median value of about 0.05 m^{-1} further than about 10 km from the coast. Elevated absorption by CDOM was associated predominantly with elevated TSM (Figure 11-7, Figure 11-8). Higher values of CDOM absorption sometimes occurred when chl-a was elevated (Figure 11-3) but sometimes did not (Figure 11-1, Figure 11-4).

8. Based on the dataset assembled here, there has been no long-term increase or decrease in TSM concentration, chl-a concentration or CDOM absorption at the 5 selected sites in the STB during the period 2002 to 2012.

8 Acknowledgements

Satellite imagery was provided by NASA Ocean Biology Processing Group. Thanks to the captain(s) and crews of the TTR validation voyages aboard R.V. Ikatere, Fiona Elliot (NIWA - Wellington) for assisting with collecting samples and underway data, Chris Cunningham and Helena Campbell (NIWA - Christchurch) for assisting with processing discrete pigment, absorption and suspended particulate samples, Simon Wood (NIWA - Wellington) for SeaDAS support and Alison MacDiarmid (NIWA - Wellington) for project leadership.

9 References

Balch, W.M., et al. (1991). Biological and optical properties of mesoscale coccolithophore blooms in the Gulf of Maine. Limnol. Oceanogr. 36(4), 629-643.

Balch, W.M. (2010). MODIS PIC algorithm (mod 23). NASA MODIS meeting 26 January 2010. Available from: modis.gsfc.nasa.gov/sci_team/meetings/201001

Bissett, W.P.; J.S. Patch; K.L. Carder; Z.P. Lee (1997). Pigment packaging and Chl a-specific absorption in high-light oceanic waters. Limnol. Oceanog. 42(5), 961 – 968.

Bowman, M.J. et al., (1983). Circulation and mixing in greater Cook Strait, New Zealand. Oceanologica Acta 6(4), 383 – 391.

Bricaud, A.; M. Babin; A. Morel; H. Claustre (1995). Variability in the chlorophyll-specific absorption coefficients of natural phytoplankton: analysis and parametrisation. J. Geophys. Res. 100: 13321–13332.

Bricaud, A.; Morel, A.; Prieur, L. (1981). Absorption by dissolved organic matter of the sea (yellow substance) in the UV and visible domains. Limnol. Oceanogr., 26(1): 43–53.

Clark, D.K. (1997). MODIS Algorithm Theoretical Basis Document – Bio-optical algorithms – Case I waters. NASA, http://oceancolor.gsfc.nasa.gov/DOCS/atbd_mod18.pdf.

Davies-Colley, R.J.; W.N. Vant; D.G. Smith (2003). Colour and Clarity of Natural Waters: Science and management of optical water clarity. The Blackburn Press.

Doerffer R.; Schiller, H. (2007). The MERIS Case 2 water algorithm. International Journal of Remote Sensing, 28(3-4): 517-535.

Falkowski, P. G., and J. A. Raven. 1997. Aquatic Photosynthesis. Blackwell Science, Inc.

Garver, S.A.; Siegel,D.A. (1997). Inherent optical property inversion of ocean color spectra and its biogeochemical interpretation: I. Time series from the Sargasso Sea. J. Geophys. Res., 102: 18,607-18,625.

Geider, R. J., H. L. Macintyre, and T. M. Kana. 1997. Dynamic model of phytoplankton growth and acclimation: Responses of the balanced growth rate and the chlorophyll a:carbon ratio to light, nutrient-limitation and temperature. Marine Ecology Progress Series 148: 187-200.

Gordon, H.R. (1997). Atmospheric correction of ocean colour imagery in the Earth Observing system era. Journal of Geophysical Research 102: 17081–17106.

Hadfield, M. (2012). Sediment Plume Modelling for South Taranaki Bight Ironsand Mining. Phase 3 interim report prepared for Trans-Tasman Resources Ltd, October 2012. NIWA Client Report: WLG2012-51, 52pp.

Hoge, F.; P. Lyon; R. Swift; J. Yungel; M. Abbott; R. Letelier; W. Esaias (2003). Validation of Terra-MODIS phytoplankton chlorophyll fluorescence line height: I. Initial airborne lidar results, Appl. Opt., 42(14): 2767–2771.

Hu, C.; Muller-Karger, F.; Taylor, C.; Carder, K.L.; Kelble, C.; Johns, E.; Heil, C. (2005). Red tide detection and tracing using MODIS fluorescence data: A regional example in SW Florida coastal waters. Remote Sensing of Environment 97(3): 311-321.

Jeffrey, S.W.; Mantoura, R.F.C; Wright, S.W. (1997). Phytoplankton pigments in oceanography. Guidelines to modern methods. Unesco Publishing, ISBN: 9231032755.

Jerlov, N.G. (1974). Optical aspects of oceanography. Academic Press, ISBN: 0123849500.

Kirk, J.T.O. (2011). Light and photosynthesis in aquatic ecosystems, Third ed. Cambridge University Press.

Lavender, S.J.; M.H. Pinkerton; G.F. Moore; J. Aiken; D. Blondeau-Patissier. (2005). Modification to the atmospheric correction of SeaWiFS ocean colour images over turbid waters. Continental Shelf Research 25(4): 539-555.

Lee, Z.P.; K.L. Carder; R.A. Arnone (2002), Deriving inherent optical properties from water color: A multi- band quasi-analytical algorithm for optically deep waters, Applied Optics, 41: 5755- 5772.

Lee, Z.P.; B. Lubac; J. Werdell; R. Arnone (2009). An Update of the Quasi-Analytical Algorithm (QAA_v5). Open file online at: http://www.ioccg.org/groups/Software_OCA/QAA_v5.pdf, 9 pp., 2009.

Letelier, R.M.; M.R. Abbott (1996). An analysis of chlorophyll fluorescence algorithms for the Moderate Resolution Imaging Spectrometer (MODIS), Remote Sens. Environ., 58(2), 215–223, doi:10.1016/S0034-4257(96)00073-9.

MacDonald, I.; M. Gall; D. Bremner (2013) Nearshore Optical Water Quality in the South Taranaki Bight. NIWA client report HAM2013-040 prepared for TransTasman Resources. Pp 88.

Macintyre, H. L., T. M. Kana, T. Anning, and R. J. Geider. 2002. Photoacclimation of photosynthesis irradiance response curves and photosynthetic pigments in microalgae and cyanobacteria. Journal of Phycology 38: 17-38.

McKibben, S.M.; Strutton, P.G.; Foley, D.G.; Peterson, T.D.; White, A.E. (2012). Satellite-based detection and monitoring of phytoplankton blooms along the Oregon coast. Journal of Geophysical Research: Oceans, 117(C12).

Mobley, C.D. (1994). Light and Water: Radiative Transfer in Natural Waters. Academic Press. ISBN-10: 0125027508.

Morel, A.; B. Gentili (2009). A simple band ratio technique to quantify the colored dissolved and detrital organic material from ocean color remotely sensed data. Remote Sensing of Environement, 113: 998-1011, doi:10.1016/j.rse.2009.01.008.

Morel, A.; L Prieur (1977). Analysis of variations in ocean color. Limnol. Oceanogr. 22: 709–722.

Mueller, J.L., et al. (2002). Ocean optics protocols for satellite ocean colour sensor validation, Revision 3, NASATech. Memo. 210004, In J.L. Mueller & G.S. Fargion (Eds.), NASA Goddard Space Flight Center, USA.

O'Reilly, J.E.; S. Maritorena; B.G. Mitchell; D. Siegel; K.L. Carder; S. Garver; M. Kahru; C. McClain (1998). Ocean color chlorophyll algorithms for SeaWiFS. J. Geophys. Res., 103(C11), 24,937, doi:10.1029/98JC02160.

Pinkerton, M.H.; G.F. Moore; S.J. Lavender; M.P. Gall; K. Oubelkheir; K.M. Richardson; P.W. Boyd; J. Aiken (2005). Intercomparison of ocean colour band-ratio algorithms for chlorophyll concentration in the Subtropical Front east of New Zealand. Rem. Sens. Env., 97(3): 382-402.

Pinkerton, M.H.; G.F. Moore; S.J. Lavender; M.P. Gall; K. Oubelkheir; K.M. Richardson; P.W. Boyd; J. Aiken. (2006). A method for estimating inherent optical properties of New Zealand continental shelf waters from satellite ocean colour measurements. New Zealand Journal of Marine and Freshwater Research 40: 227–247.

Ruddick, K.G.; Ovidio, F.; Rijkeboer, M. (2000). Atmospheric correction of SeaWiFS imagery for turbid and inland waters. Applied Optics, 39: 897-912.

Shanmugam, P. (2011). A new bio-optical algorithm for the remote sensing of algal blooms in complex ocean waters. Journal of Geophysical Research 116 (C4): C04016.

Stramski. D.; R.A. Reynolds; M. Babin; S. Kaczmarek; M.R. Lewis; R. Rottgers; A. Sciandra; M. Stramska; M.S. Twardowski; B.A. Franz; H. Claustre (2008). Relationships between the surface concentration of particulate organic carbon

and optical properties in the eastern South Pacific and eastern Atlantic Oceans, Biogeosci., 5: 171-201.

Strickland, J.D.H.; Parsons, T.R. (1972). A practical handbook of seawater analysis. Fisheries Board of Canada, ISBN 0660115964.

Tassan, S.; Ferrari, G.M. (1995). An alternative approach to absorption measurements of aquatic particles retained on filters. Limnol. Oceanogr. 40(8): 1358-1368.

Wang, M.; Shi, W. (2007). The NIR-SWIR combined atmospheric correction approach for MODIS ocean color data processing. Optics Express, 15(24): 15722-15733, http://dx.doi.org/10.1364/OE.15.015722.

Zapata, M.; Rodriguez, F.; Garrido, J.L. (2000). Separation of chlorophylls and carotenoids from marine phytoplankton: a new HPLC method using a reversed phase C8 column and pyridine- containing mobile phases. Mar. Ecol. Prog. Ser., 95: 29-45.

10 Appendix A: Satellite data coverage

The numbers of data points used in the annual compilations for total suspended sediment (Figure 4-1), chlorophyll-a concentration (Figure 5-1) and detrital absorption (Figure 6-1) are shown below in Figure 10-1, Figure 10-2 and Figure 10-3 (respectively). The striping is caused by the way satellite data (at oblique views) were mapped onto the regular latitude-longitude output grid.

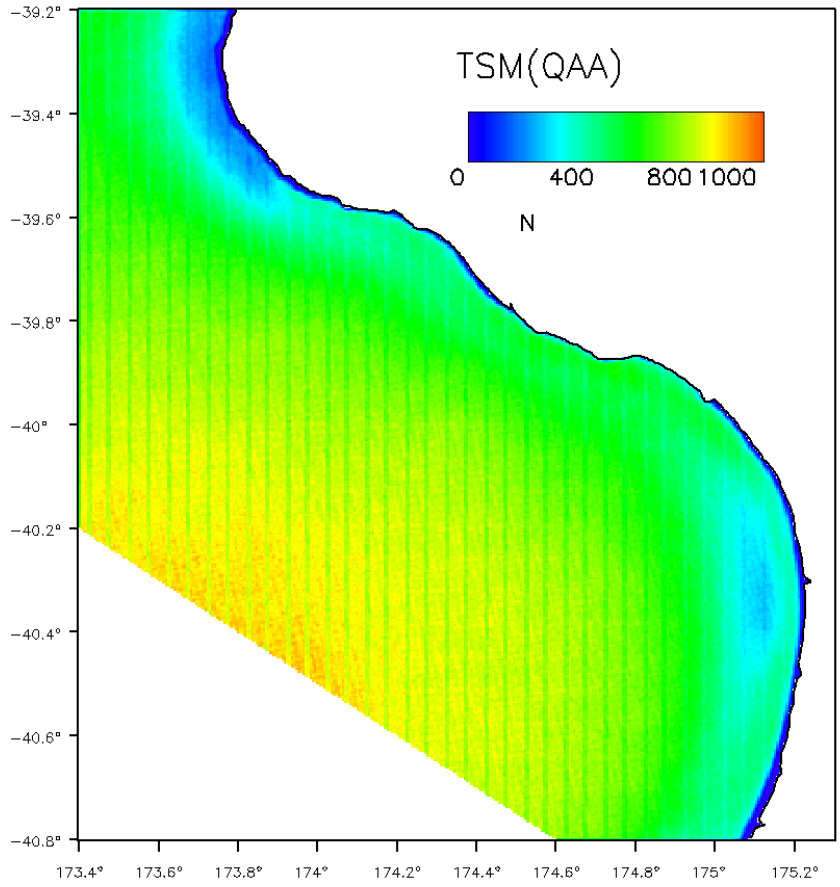

Figure 10-1: Number of particulate backscatter (BBP488) data points used in generating Figure 4-1.

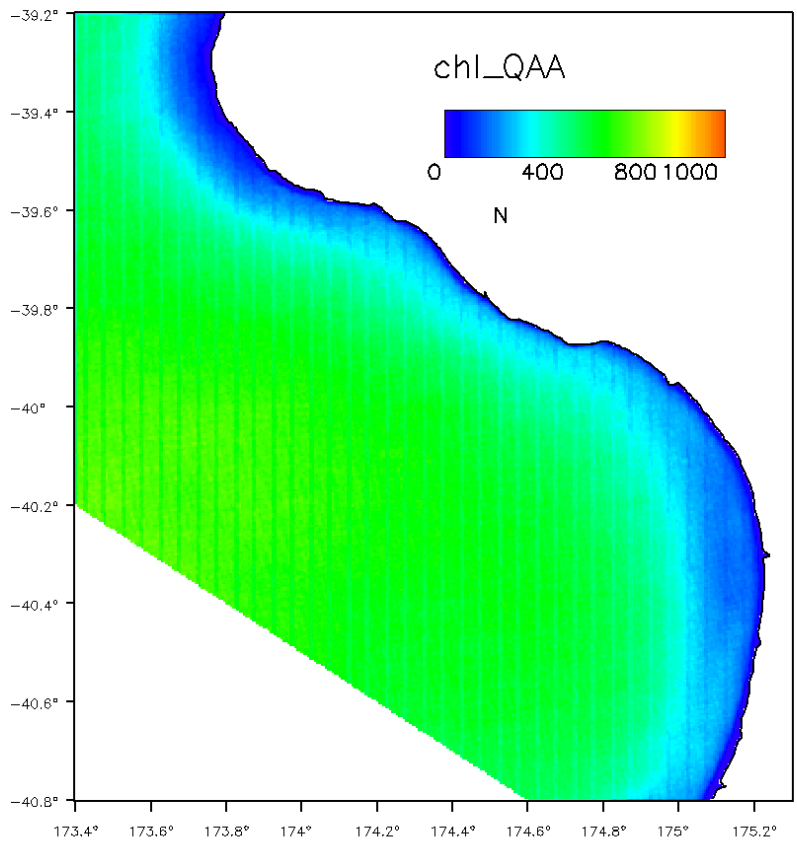

Figure 10-2: Number of algal absorption (APH488) data points used in generating Figure 5-1.

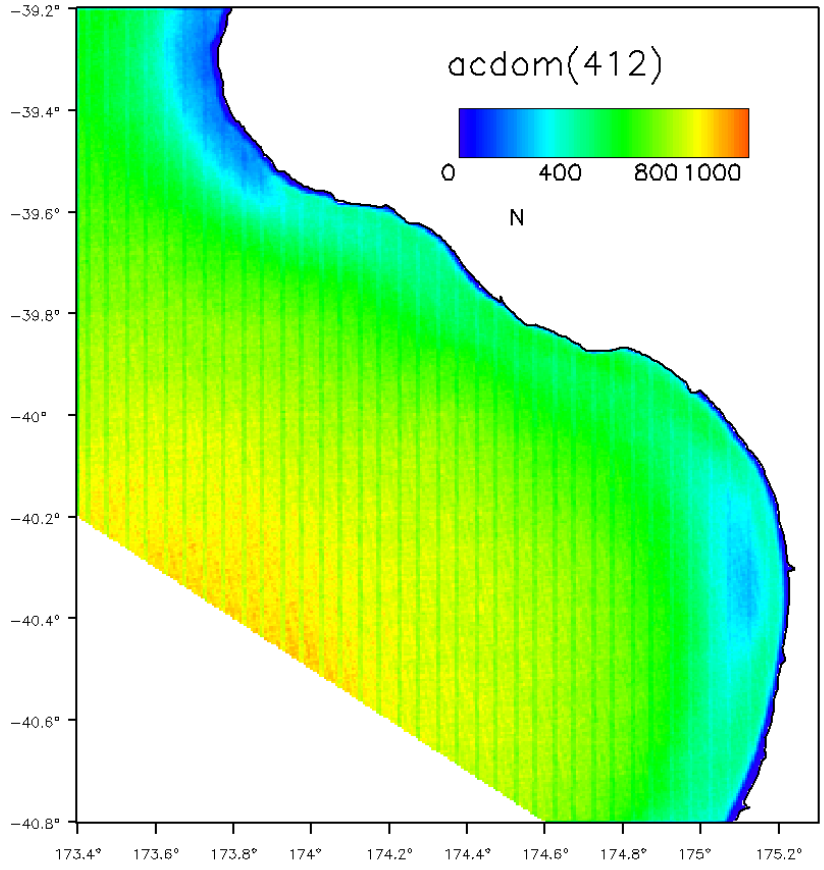

Figure 10-3: Number of detrital absorption (ADET412) data points used in generating Figure 6-1.

11 Appendix B: Satellite images from selected days to illustrate features

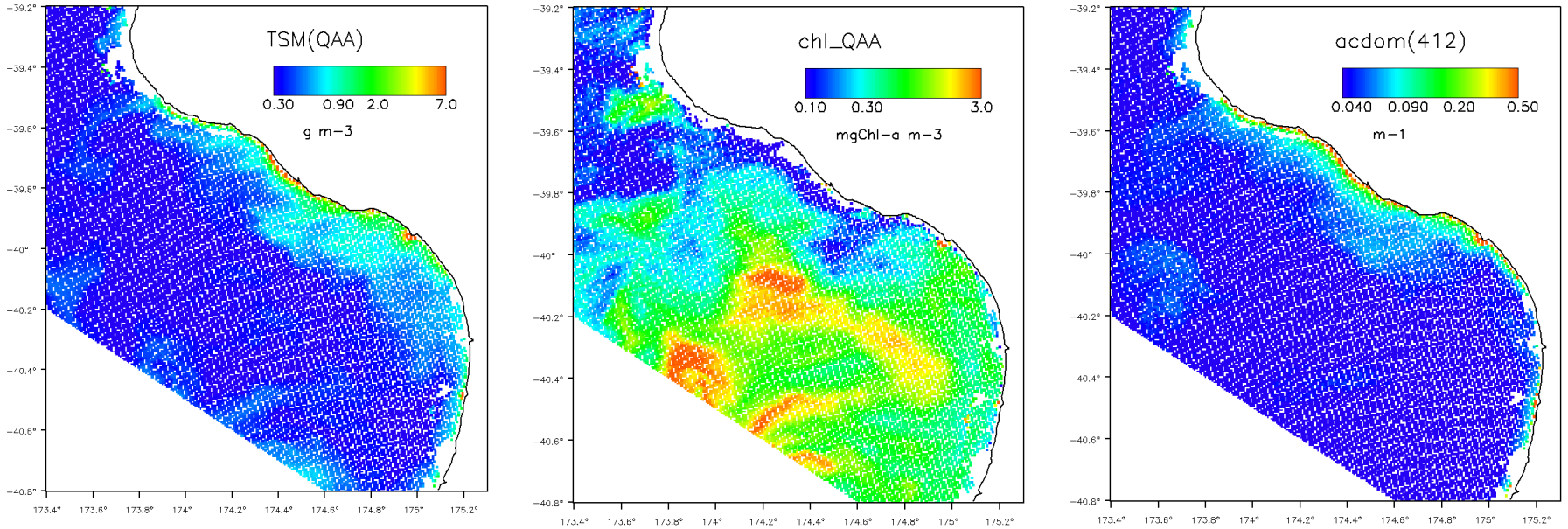

Figure 11-1: Offshore phytoplankton blooms (chl-a in middle of bloom ~4 mg m^{-3}). [A2002336023000 – MODIS-Aqua products: left: total suspended matter (TSM); middle: chl-a; right: CDOM absorption at 412 nm (QAA algorithm).]

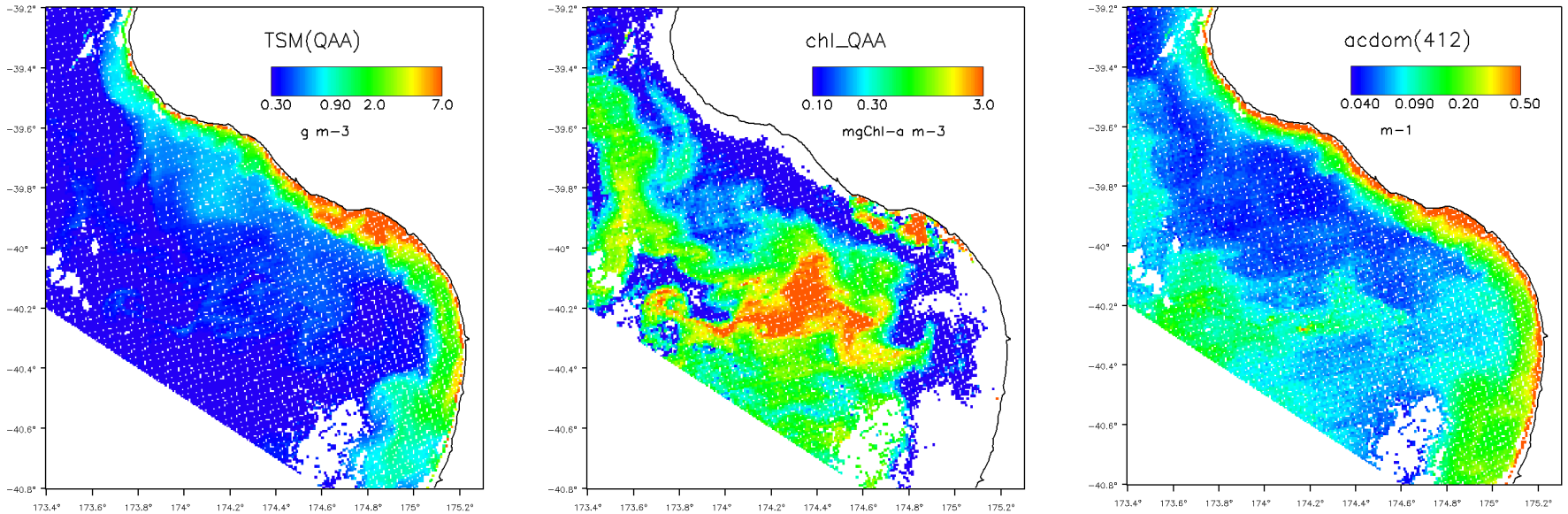

Figure 11-2: Offshore phytoplankton blooms (chl-a in middle of bloom ~4 mg m^{-3}). [A2006340023000 – MODIS-Aqua products: left: total suspended matter (TSM); middle: chl-a; right: CDOM absorption at 412 nm (QAA algorithm).]

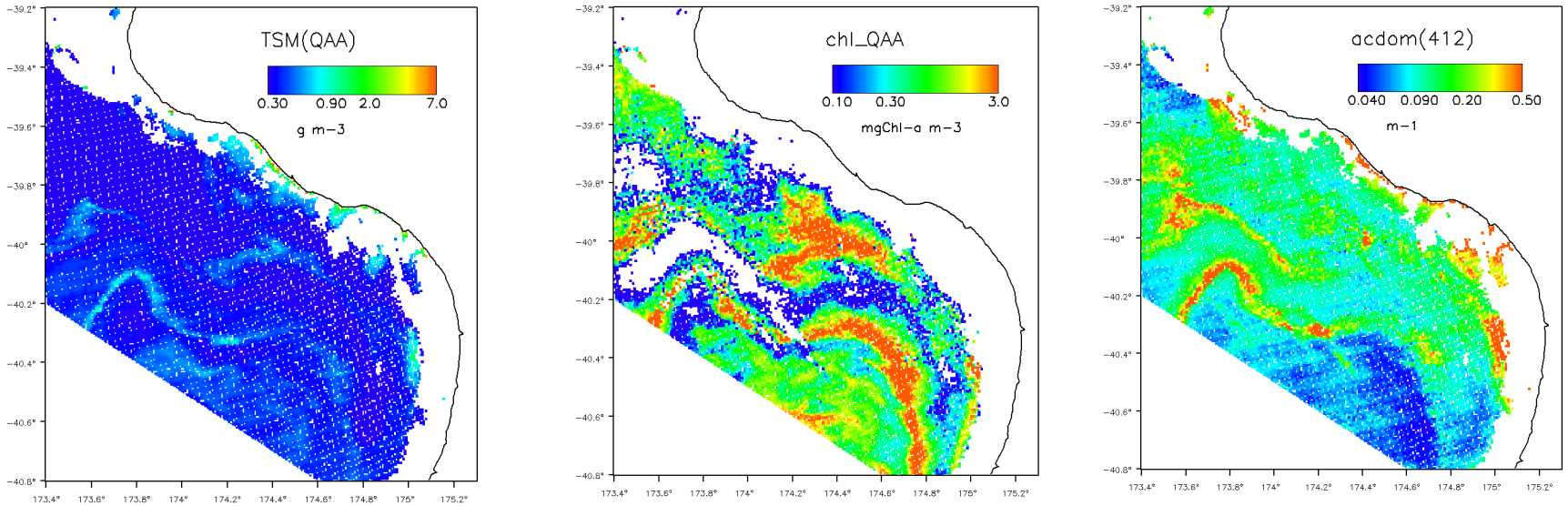

Figure 11-3: Large filamented offshore phytoplankton blooms (chl-a in middle of bloom ~4 mg m^{-3}). [A2007263023000 – MODIS-Aqua products: left: total suspended matter (TSM); middle: chl-a; right: CDOM absorption at 412 nm (QAA algorithm).]

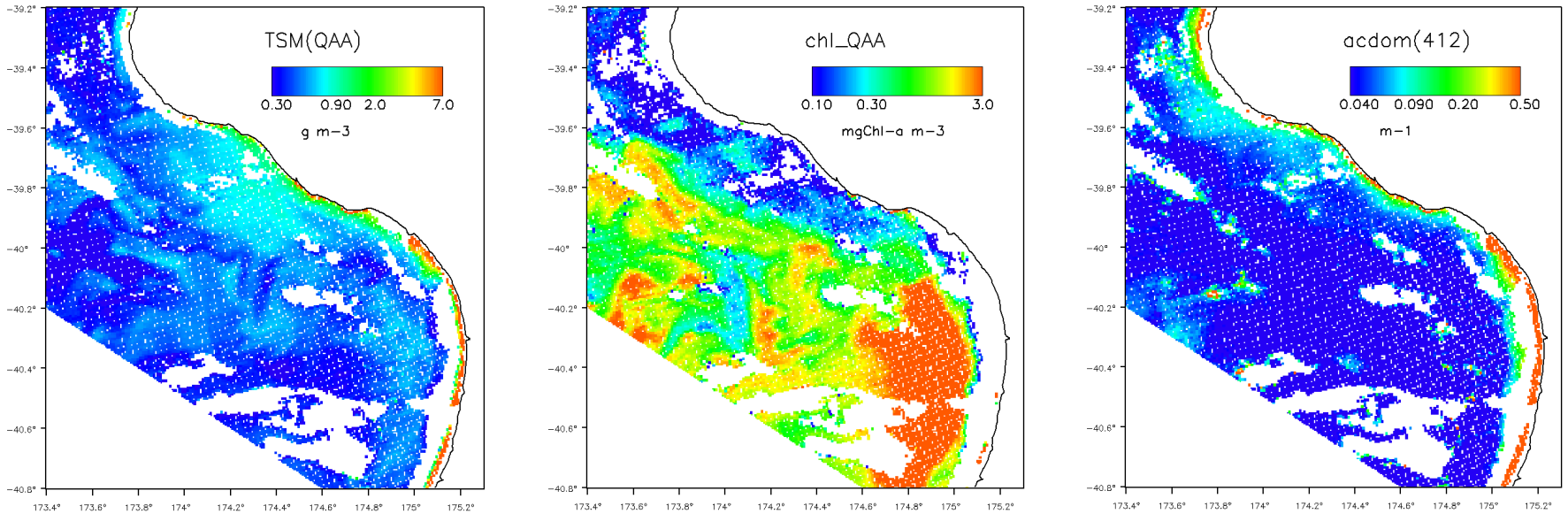

Figure 11-4: Phytoplankton bloom in southern part of STB (chl-a in middle of bloom ~8 mg m^{-3}). [A2005289022500 – MODIS-Aqua products: left: total suspended matter (TSM); middle: chl-a; right: CDOM absorption at 412 nm (QAA algorithm).]

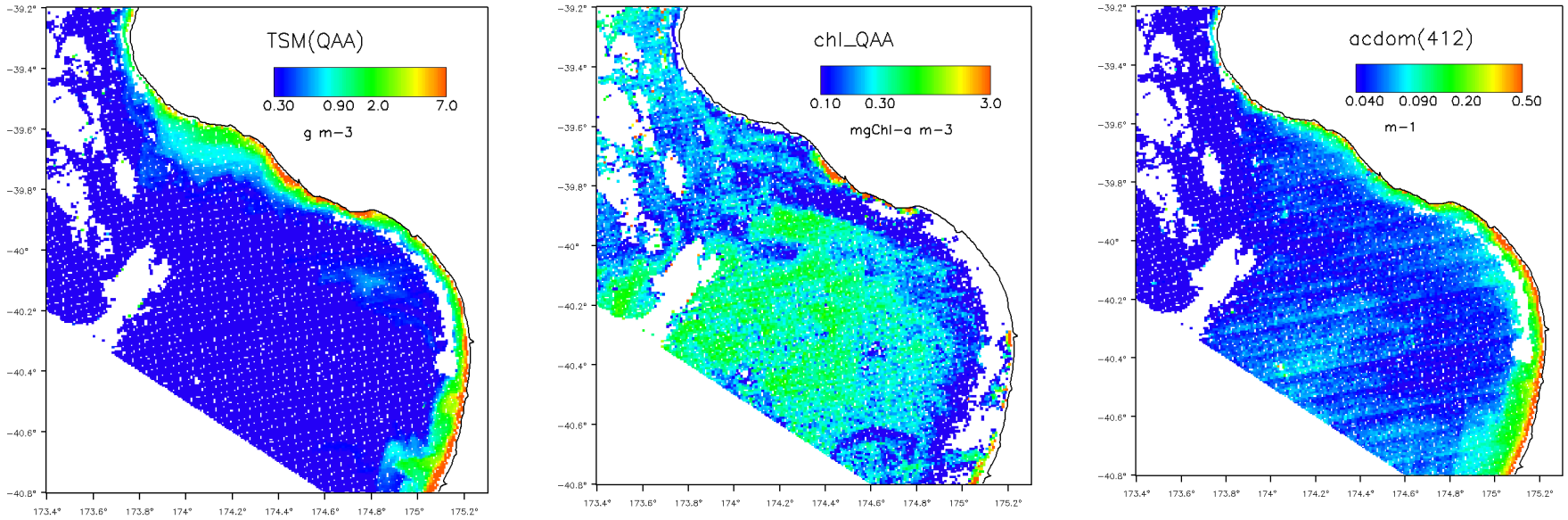

Figure 11-5: "Blue water" - low coastal sediment and phytoplankton. [A2008115022000– MODIS-Aqua products: left: total suspended matter (TSM); middle: chl-a; right: CDOM absorption at 412 nm (QAA algorithm).]

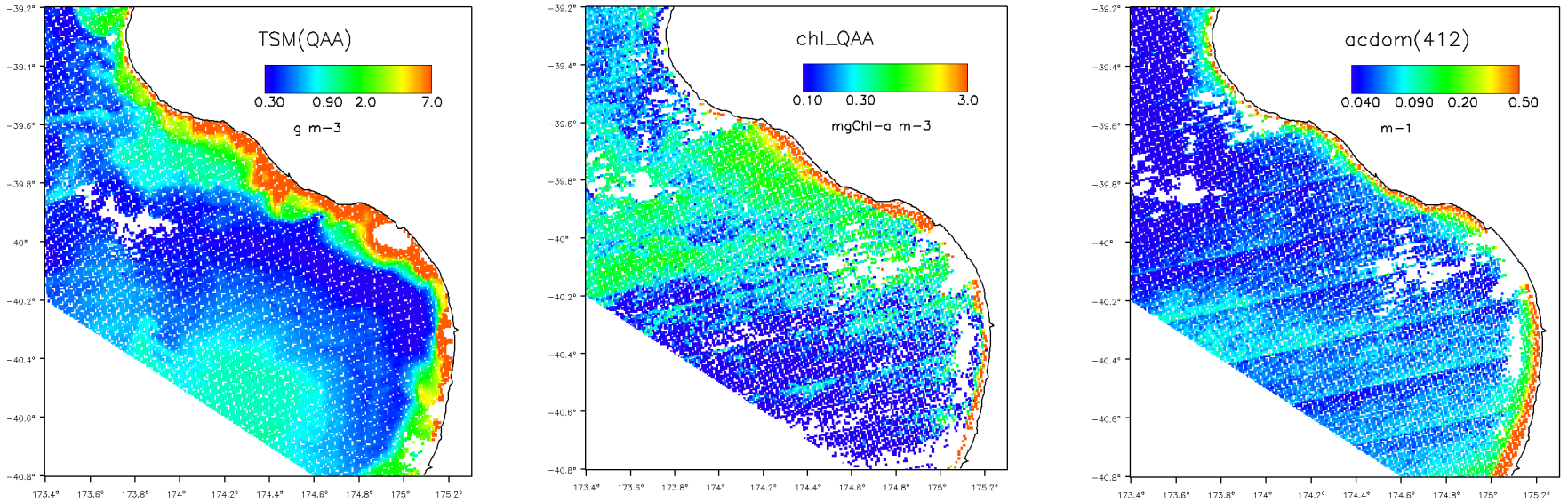

Figure 11-6: High coastal sediment loads in STB. [A2009206022000 – MODIS-Aqua products: left: total suspended matter (TSM); middle: chl-a; right: CDOM absorption at 412 nm (QAA algorithm).]

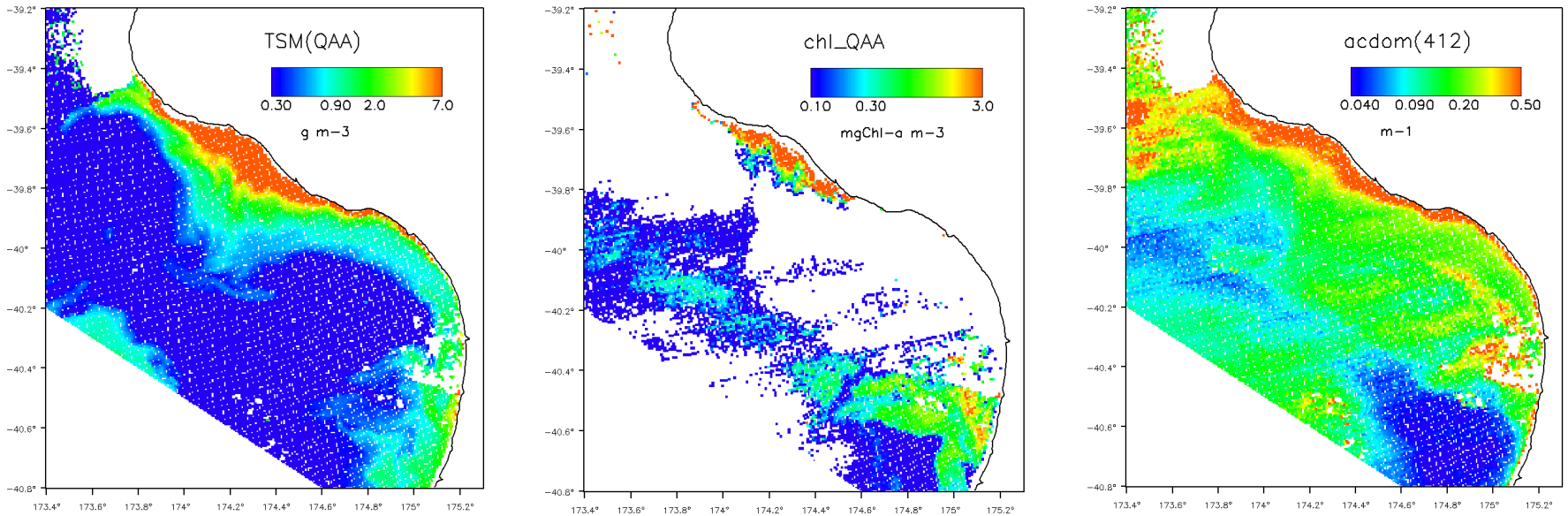

Figure 11-7: High coastal sediment loads in north of STB. [A2012069023000 – MODIS-Aqua products: left: total suspended matter (TSM); middle: chl-a; right: CDOM absorption at 412 nm (QAA algorithm).]

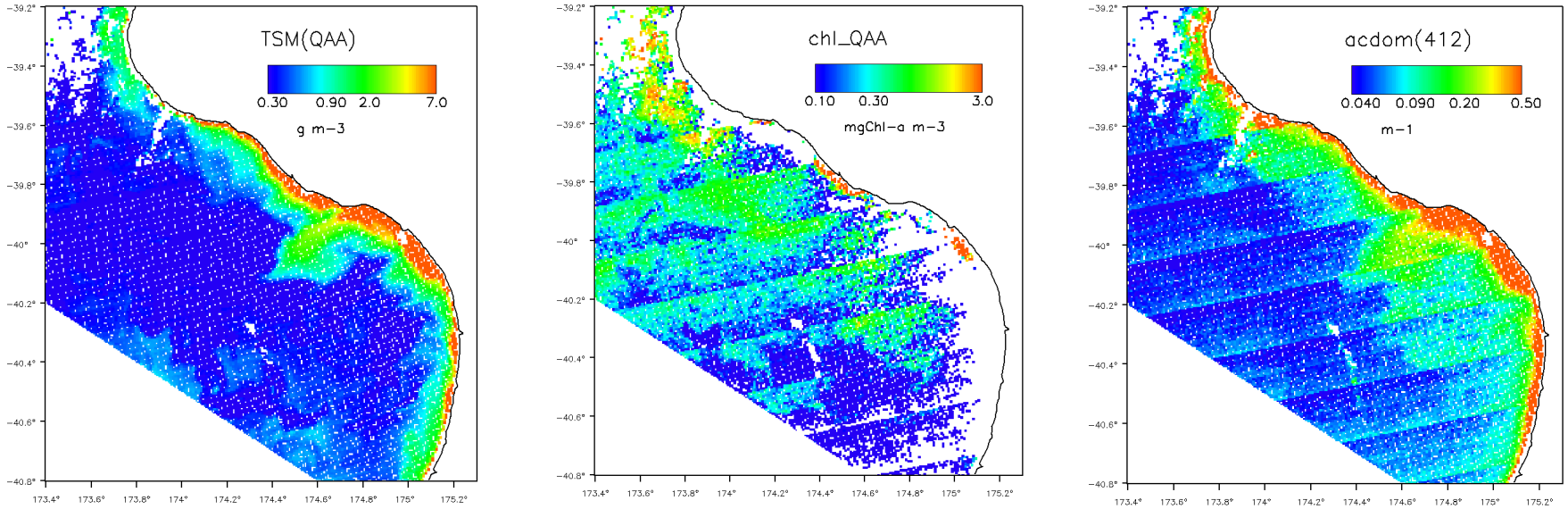

Figure 11-8: Coastal sediment being transported offshore. [A2010223023000 – MODIS-Aqua products: left: total suspended matter (TSM); middle: chl-a; right: CDOM absorption at 412 nm (QAA algorithm).]

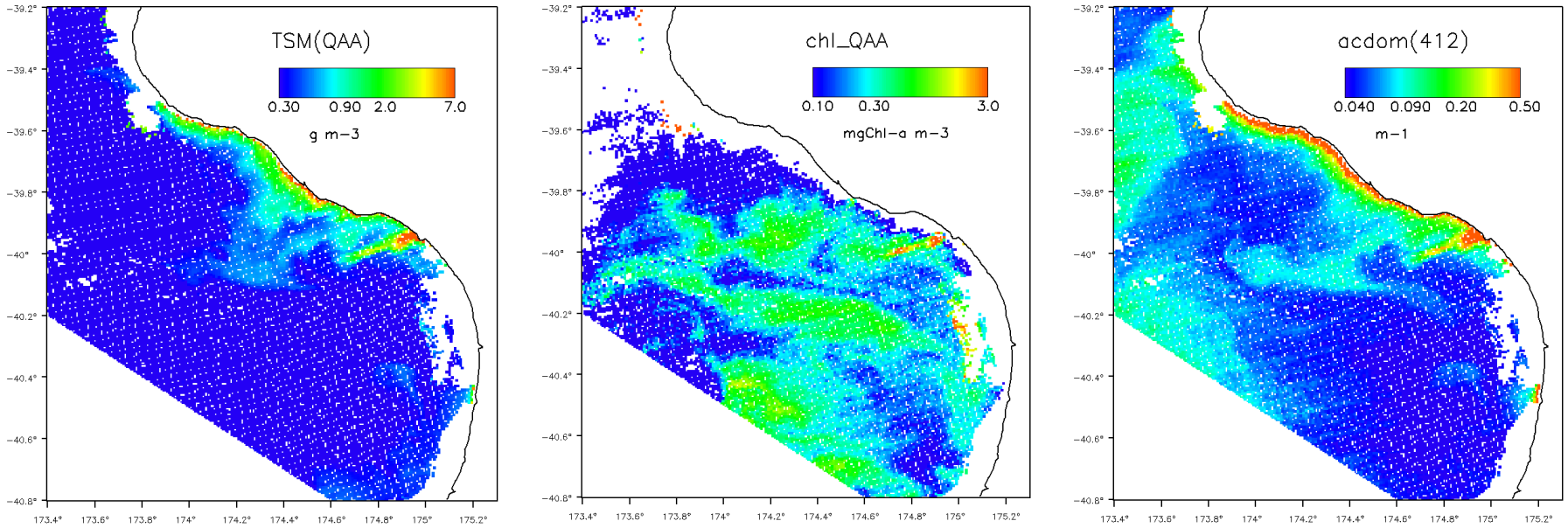

Figure 11-9: Coastal sediment being transported offshore. [A2011354023000 – MODIS-Aqua products: left: total suspended matter (TSM); middle: chl-a; right: CDOM absorption at 412 nm (QAA algorithm).]